Synsint Research Group

Available online at www.synsint.com

Synthesis and Sintering

ISSN 2564-0186 (Print), **ISSN** 2564-0194 (Online)

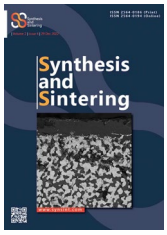

Review article

New strategies in the preparation of binary g-C_3N_4/MXene composites for visible-light-driven photocatalytic applications

Asieh Akhoondi [a,*], **Mehrdad Mirzaei** [b,*], **Mostafa Y. Nassar** [c], **Zahra Sabaghian** [d], **Farshid Hatami** [e], **Mohammad Yusuf** [f,g]

[a] *Department of Chemical Engineering, Arak Branch, Islamic Azad University, Arak, Iran*
[b] *Nanomaterials Group, Department of Materials Engineering, Tarbiat Modares University, P.O. Box 14115-143, Tehran, Iran*
[c] *Chemistry Department, Faculty of Science, Benha University, Benha, 13518, Egypt*
[d] *Department of Chemical Engineering, Faculty of Engineering, Ferdowsi University of Mashhad, Mashhad, Iran*
[e] *Chemical and Material Engineering Department, Esfarayen University of Technology, Esfarayen, Iran*
[f] *Department of Petroleum Engineering, Universiti Teknologi PETRONAS, Bandar Seri Iskandar, Perak, 32610, Malaysia*
[g] *Institute of Hydrocarbon Recovery, Universiti Teknologi PETRONAS, Bandar Seri Iskandar, Perak, 32610, Malaysia*

ABSTRACT

In recent years, g-C_3N_4@MXene photocatalysts have received much attention due to their special composition and excellent properties. MXenes consisting of transition metal carbides, nitrides, and carbonitrides derived from the MAX phase are used as cocatalysts or g-C_3N_4 (GCN) supporting composites in a variety of photocatalytic processes that accelerate the separation of charge carriers with their heterojunction structure. In addition to the high ability of g-C_3N_4@MXene nanocomposite to absorb light, it has high photocorrosion resistance in the processes of hydrogen evolution, wastewater treatment, nitrogen fixation, NO treatment, and oxidation and reduction photoreactions. In this review, the latest developments and new technologies for the manufacture and application of noble metal-free g-C_3N_4@MXene nanocomposite have been discussed and the future perspective has been drawn to deal with challenges related to energy and the environment.

KEYWORDS

Photocatalyst
g-C_3N_4
MXene
Synthesis
Nanocomposite

OPEN ACCESS

1. Introduction

The global growth of carbon fossil fuels consumption in the recent century has led to increasing concerns about the depletion of this non-renewable source of energy. In terms of statistics, 1.5 billion tons have been added to the global carbon emissions this year, and the risk of CO_2 greenhouse gas emissions has reached its highest level as indicated in the report of the International Energy Agency. Consequently, with the actual increase in energy crises and environmental pollution, it is necessary to develop new technologies to solve these challenges. The rise in population coinciding with the extension of industries has fueled the expansion of these problems. Therefore, in developed and developing countries, researchers are looking for appropriate solutions with a scale-up approach for industrialization. In this regard, sunlight as an infinite and free source of energy has a high alternative potential for oil and gas and can also be used in various chemical industries. Hydrogen production from solar energy that is independent of any non-renewable fossil resources is one of the promising solutions for fuel replacement. Photocatalysis technology based on the absorption of solar radiation by a catalyst named photocatalyst, which is mainly a semiconductor, has been investigated in the fuel supply area and environmental applications in the last three decades [1–4].

* Corresponding author. *E-mail address:* asieh.akhoondi@gmail.com (A. Akhoondi), mehrdad.mirzaie@modares.ac.ir (M. Mirzaei)
Received 29 August 2022; Received in revised form 25 December 2022; Accepted 25 December 2022.

https://doi.org/10.53063/synsint.2022.24121

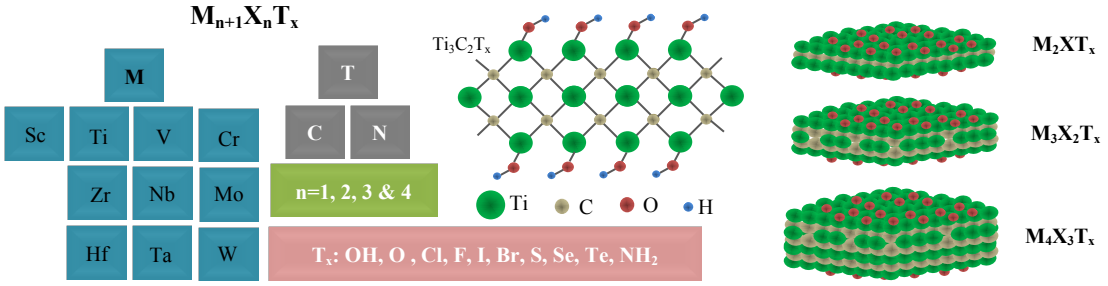

Fig. 1. Schematic of Maxine's general formula and $Ti_3C_2T_x$ structure.

The design and preparation of photocatalysts that can use a broad spectrum of light to produce green fuel instead of fossil fuels and break down water and air pollutants are expanding. In photocatalysis, chemical reactions occur in a system containing a mostly heterogeneous catalyst capable of absorbing visible or ultraviolet light. This idea originates from the process of photosynthesis, and various semiconductors such as oxides, sulfides, etc. are used as photocatalysts. A photocatalyst can provide a platform for difficult or impossible reactions, but at the end of the reaction, it remains unchanged and can be reused. Photocatalytic technology can be used in renewable green energy storage instead of coal, oil, or natural gas by light illumination, thus avoiding environmental damage. Moreover, photocatalysis can be exploited in specific applications such as CO_2 reduction, NO purification, N_2 fixation, H_2O_2 production, degradation of organic contaminants, photoelectrochemical conversion, etc. By absorbing photons of light, photocatalysts create charge carriers that are electron-hole (e^-/h^+) pairs. These photoinduced electron-hole pairs transfer to the semiconductor surface and drive the redox reaction. Undoubtedly, the choice of photocatalyst and its morphology plays an essential role in light harvesting and photocatalytic efficiency. Therefore, photocatalyst characteristics, including the ability to transport charge carriers, specific surface area, light absorption, and reflection, affect photocatalytic performance [5–11].

Graphite carbon nitride (GCN) is a polymer material in which carbon and nitrogen atoms are connected by double-bonded. The unique features of this material, including the ease of synthesis (condensation polymerization of urea or melamine) stability in very acidic and basic environments, and suitable bandgap, have stimulated various research groups to focus on its photocatalytic properties for producing hydrogen and oxygen from water as well as the destruction of pollutants. Synthesized graphitic carbon nitride has a favorable ability for photocatalytic degradation of organic materials [12]. Graphite carbon nitride is one of the semiconductors that have a smaller gap band compared to other common photocatalysts such as titanium oxide and zinc oxide, and as a result, the efficiency of this material to absorb sunlight is higher [13]. Therefore, it is a recommended for replacing photocatalysts based on metal oxide, which has a higher efficiency compared to this category of semiconductors. Regardless, efforts have been made to optimize its photoelectric properties, and increase visible spectrum absorption and charge separation efficiency [14]. Therefore, several experiments have been designed to increase the efficiency of g-C_3N_4 by making binary or ternary composites with compounds such as $BiVO_4$, $InVO_4$, $AgVO_3$, V_2O_5, TiO_2, and ZnO [15–19]. Another strategy that has been significantly explored is the non-metallic elemental doping of O, S, N, and P, which are used as cocatalysts. GCN is widely used in hydrogen production, wastewater treatment, organic dye removal, and CO_2 reduction [20, 21]. Recently, two-dimensional cocatalysts MXenes are used to enhance the photocatalytic performance of GCN in these photocatalytic applications.

MXenes are emerging group of transition metal carbide/nitride two-dimensional materials prepared from MAX phases which have a tremendous effect on photocatalytic processes [22, 23]. The most famous MXene is $Ti_3C_2T_x$, whose molecular structure is shown in Fig. 1. The high contact surface of these nanomaterials increases the absorption efficiency [24]. In general, 2D materials are limited to one or to a few atoms in one dimension (typically less than 5 nm) and can be over 100 nm to a few micrometers in the other dimension. Accordingly, the contact surface of two-dimensional materials has increased significantly, which enhances their reaction rate and affects their performance wave in the quantum field. As a result, these structures have unique catalytic, electronic, photonic, and magnetic natures that are different from their bulk counterparts. The emergence of new 2D materials other than graphene, in addition to focusing on new discoveries in photocatalysis, has shown their tremendous potential applications for diverse technologies. MAX phases, which are also known as metal ceramics, are thermodynamically stable nano-laminates and are considered among three-component layered ceramics and have dual behaviors of the properties of metals and ceramics [25]. This group of materials has a combination of metallic properties such as high flexibility and toughness, and ceramic properties such as high elastic constant and wear resistance, low density, and good resistance to corrosion and oxidation [26]. This means that this group of materials has not only the properties of ceramics but also some useful and good properties of metals. In general, Max phases consist of $M_{n+1}AX_n$, where M is an intermediary metal, A is an element belonging to IIIA and IVA groups, and X represents nitrogen or carbon. The value of index n varies from one to three and can change depending on the composition [27]. MXene structures are made of Max phases. Max phases have three hexagonal lattice unit cell models where M layers are compactly placed between A layers and octahedral sites are filled with X atoms. Similar to max phases, MXenes have hexagonal structures and X atoms fill the octahedral positions. MXenes are very promising to be used in photocatalysis due to high specific surface area and superior mechanical and electrical properties [28, 29]. MXenes are fabricated by selectively etching layers of element A from MAX phase at room temperature [30, 31]. Fig. 2. represents synthesis approaches with morphologists obtained and a variety of photocatalytic applications of MXene/g-C_3N_4. These hybrid photocatalysts are incorporated in other

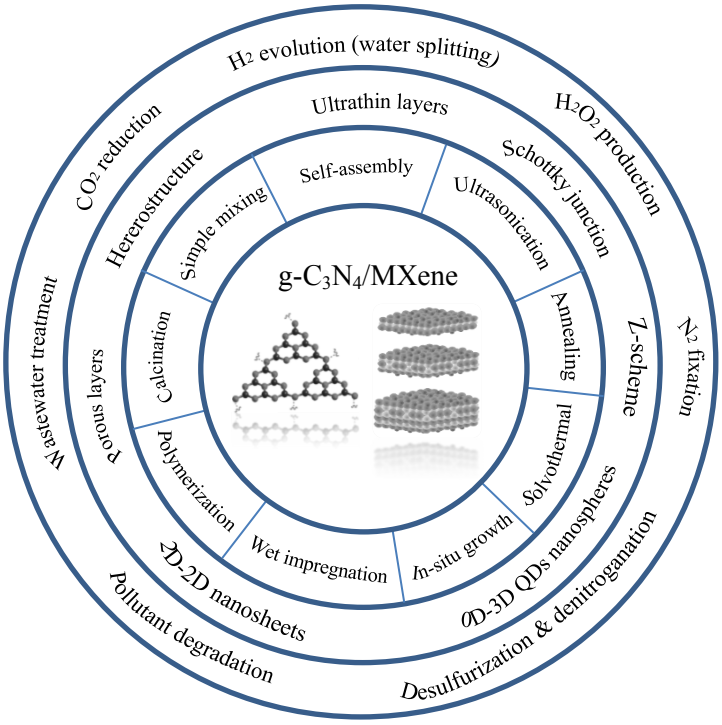

Fig. 2. Schematic representation of approaches to the fabrication, morphology and photocatalytic applications of g-C_3N_4/MXene.

applications such as solar energy absorbers, biosensors, batteries, supercapacitors, electrocatalytic reaction, cathodic protection, etc., which are mentioned in the articles [32–37].

Previously, several researchers have published reviews on the preparation and photocatalytic applications of g-C_3N_4 and MXene and composites based on these semiconductors. However, no general summary has been provided about the fabrication of binary MXene/g-C_3N_4 photocatalysts and their applications. In this review, firstly the basics and mechanism of photocatalysis have been discussed. Then, g-C_3N_4@MXene hybrid photocatalyst synthesis methods including calcination, ultrasound, mixing, self-assembly, hydro/solvothermal, in situ growth, annealing, wet impregnation, and polymerization techniques are discussed regardless of the preparation method of pristine GCN and pure MXene. In the following, the utilizations of g-C_3N_4@MXene in the field of H_2 evolution, pollutant destruction, CO_2 reduction, N_2 fixation, H_2O_2 production, and NO purification are discussed regardless of g-C_3N_4@MXene derivatives and any ternary combination thereof. Finally, the merits, weaknesses, challenges, and outlooks are described for the direction of further research.

2. Principles of photocatalysis mechanism

Photocatalytic reactions are initiated by the light absorption with suitable energy that is same as or greater than the bandgap energy of the photocatalyst. The energy gap is the distance between the conduction band (CB) and the valence band (VB) in the electronic configuration of the material. In simpler terms, the bandgap is the minimum energy required to excite an electron from the VB to the CB, where it can flow freely along preferred paths. The difference in this energy gap differentiates conductive, semi-conductive, and insulating materials. Semiconductors have a state between conductors and insulators, and electrons can escape from their VB with enough energy to participate in CB. For each transferred electron, a positively charged h^+ remains in the VB. If an e^- from a nearby atom can fill this empty space, a chain reaction between e^- and h^+ occurs, which is the basis of photocatalysis. Quantum efficiency (QE) is defined as the proportion of the numeral of created electron-holes per absorbed photon. The number of electrons and holes on the surface are not equal in reality. Therefore, dimensional changes, engineering, and surface modifications of photocatalyst materials are necessary to increase their performance. For a photocatalytic reaction to occur, it is necessary to perform these steps: 1) absorption of photons to create electron-hole pairs; 2) separation of photoexcited e^-/h^+ paires; 3) transfer of charge carriers to the semiconductor surface; 4) use of surface charges for redox reactions. In the third step, a large part of the electron-hole pairs is recombined along the path or on the surface [38]. As a result of this combination, the absorbed electron energy is released as heat or light, which reduces the efficiency of the photocatalyst. In addition to creating a thermodynamic shortcut, the photocatalyst changes the reaction pathway and thereby improves the reaction kinetics. Since all chemical reactions occur on the surface; therefore, the size of the particle and morphology of the semiconductor have a substantial effect on the surface area and consequently the reaction rate. Research has shown that nanostructured materials with dimensions less than 20 nm show distinct physical and chemical behavior compared to their bulk scale. In general, as the particle size decreases, the surface area of the photocatalyst material increases and becomes more capable of absorbing reactants and photons. Therefore, the negative effect of increasing the energy gap is somewhat neutralized in this way. The selection of semiconductors in photocatalytic processes is based on price, non-toxicity, high flexibility, and electron transfer ability [39]. Besides these items, the distance of the bandgap for absorbing light

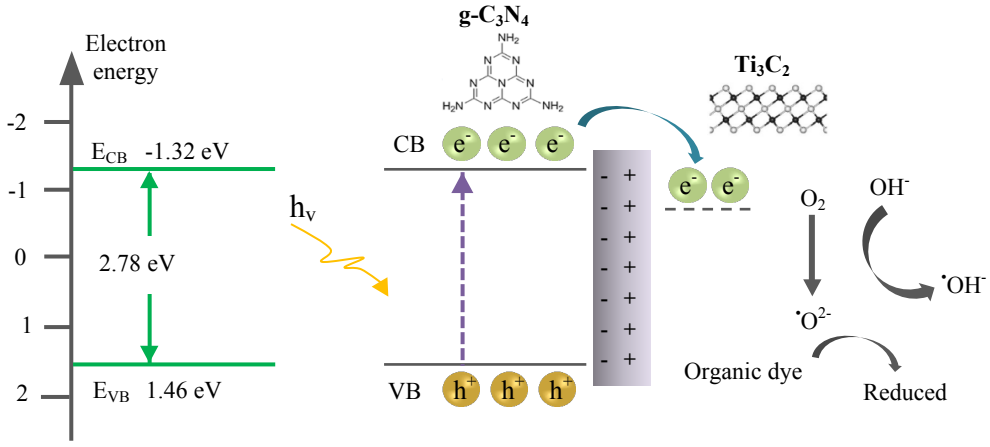

Fig. 3. Mechanism of charge carrier's transfer from g-C_3N_4 to Ti_3C_2 under light irradiation.

spectrum, the stability, and the recombination rate of electron-hole pairs also limit the choice of the photocatalyst. Fig. 3 shows a schematic diagram of electrons flow from GCN to Ti_3C_2 as a representative of MXenes.

3. Construction of binary g-C_3N_4/MXene composite

Fabrication of heterojunctions GCN@MXene nanocomposites has been studied in addition to photocatalytic applications in the electrochemical field, sensors, capacitors, and batteries [40–43]. However, high specific surface area, good dispersion, homogeneity, and mechanical strength for reuse should be considered in the synthesis of g-C_3N_4@MXene. Therefore, various synthesis methods have been studied, which are investigated below. Herein, the aim is not to focus on the synthesis procedure of pure MXene and GCN, but its generalities will be discussed briefly.

MXenes result from the selective elimination of the A layers from MAX phase structures. The general composition of the MAX phase is $M_{n+1}AX_n$, in which A appears as a metal from the third or fourth group of the periodic table. For example, the removal of Al elements from the Ti_3AlC_2 compound leads to the synthesis of $Ti_3C_2T_x$ MXene. Because the A–M bond is a strong metal connection, it must be broken by a chemical method. Aqueous solutions of hydrofluoric acid have been used for the selective removal of A. Moreover, lithium fluoride salt along with hydrochloric acid can be a suitable substitute for the highly corrosive hydrofluoric acid (HF) in the process of converting the MAX phase to MXene [44, 45].

Various methods have been used to fabricate heterojunction MXene/g-C_3N_4 nanocomposites, which provide homogeneous growth and good dispersion, and excellent mechanical stability for the prepared MXene/g-C_3N_4. These approaches are based on the MXenes as cocatalyst and stable support material due to their excellent electrical conductivity, distinctive 2D layered nanostructure, high specific surface area, great carrier mobility, and excellent hydrophilicity.

3.1. Calcination method

In the calcination method, a thermal treatment is performed on the solid, in which volatile substances and impurities are removed or decomposed under high temperatures in the desired atmosphere. Therefore, the process can also be considered thermal purification while the main materials do not melt during heating. In several studies, the calcination technique has been utilized to prepare GCN/MXene. For example, 2D/3D g-C_3N_4@Ti_3C_2 heterojunction composite has been fabricated via an in-situ one-step calcination strategy, as shown in Fig. 4 [46]. Melamine powder in distilled water has been used as a raw

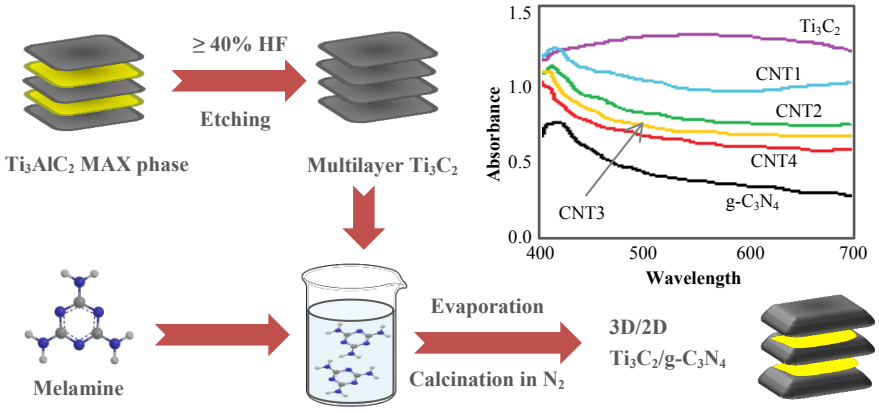

Fig. 4. Showing the fabrication steps of g-C_3N_4@Ti_3C_2 from melamine and Ti_3AlC_2.

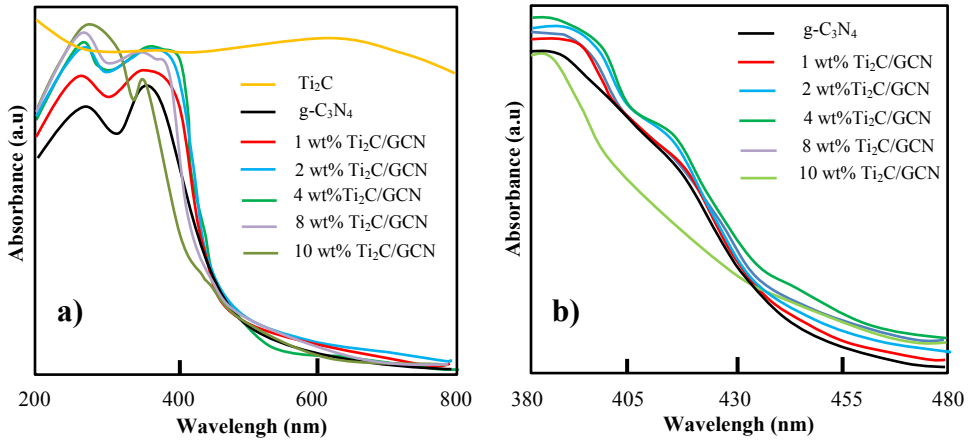

Fig. 5. a) UV-vis diffuse reflectance spectra of GCN and Ti_2C/GCN and b) magnified view of the left image at wavelengths of 380 nm to 480 nm.

material in the preparation of g-C_3N_4. The solution was stirred at a temperature higher than room temperature for several hours and then Ti_3C_2 powder was added to the suspension. After evaporation of the solvent and drying the obtained powder, the product has been subjected to heat treatment under nitrogen flow. High stability has been observed due to an effective association with g-C_3N_4 and Ti_2C. In another study, Shao et al. have loaded GCN on Ti_2C in an ethanol solution by calcination method without being oxidized [47]. The absorption spectra using UV-vis diffuse reflectance spectra, as an important testing of photocatalysts, show improvement in visible light absorption (Fig. 5). Urea can also be used as a polymeric C_3N_4 precursor in the presence of an alkaline solution for $Ti_3C_2T_x$ hybridization by co-calcination method [48]. It is reported that the interlayer spacing of Ti_3C_2 under heat treatment in ammonia atmosphere increases while the number of –F functional groups decreases. As described by Yang et al., urea can play two main roles during in situ calcination, both as a precursor for g-C_3N_4 nanosheets (NSs) and as a template gas for Ti_3C_2 exfoliation into nanosheets [49]. With the ultrasonic dispersion of concentrated urea in Ti_3C_2, urea molecules penetrate the layers and due to the limitation of Ti_3C_2 by terminated group, urea penetrates the surface. In another research, melamine and HNO_3 as precursors have been used to prepare g-C_3N_4/Mo_2C hybrid photocatalysts [50]. However, Mo_2C NPs have been combined with nanorod-like GCN to fabricate Mo_2C/g-C_3N_4 using freeze-drying and calcination methods. It has been found that Mo_2C has a positive impact on improving the optical effects of GCN due to the stronger ability of Mo_2C/GCN for photon harvesting compared with bulk GCN in the UV-Vis diffuse reflectance spectra. However, Mo_2C does not diffuse into g-C_3N_4 crystal lattice, so it does not change the light absorption edge [51]. For photocatalytic nitrogen fixation, Sun et al. designed 2D/2D Ti_3C_2/N-defect GCN heterostructure [52]. They have used citric acid to introduce N defects into GCN to anchor Ti_3C_2 through electrostatic adsorption on N defects. The –O ending groups can fill the N-defects by the calcination process in N_2, hence the Ti–O–C bond forms as a charge transfer pathway between Ti_3C_2 and GCN.

3.2. Ultrasonication method

The principle of the ultrasonication method involves the transmission of ultrasound waves through a liquid medium, and then microbubbles are formed, grow, and burst in the solution. This method is used to distribute nanomaterials in different compositions. Direct hybridization of g-C_3N_4 and Ti_3C_2 by the simple pathway of ultrasonication forms good interaction between GCN and MXene layers [53]. For a typical preparation, the appropriate amount of g-C_3N_4 has been introduced to Ti_3C_2 in dimethyl sulfoxide solution, agitated for 24 h, and then treated by ultrasound waves for 60 min to obtain g-C_3N_4/Ti_3C_2 layers. After an ultrasonic stirring process, a heterojunction structure has been established between the porous GCN and Ti_3C_2 phases followed by the straightforward vacuum filtration [54]. In another examination, Zeng et al. have prepared GCN/$Ti_3C_2T_x$ through an ultrasound method to construct a hydrophilic and antifouling composite membrane [55]. For this purpose, GCN and MXene precursors have been supplied separately (Fig. 6). $Ti_3C_2T_x$ as a cocatalyst can improve the recyclability of GCN during the wastewater treatment and elimination

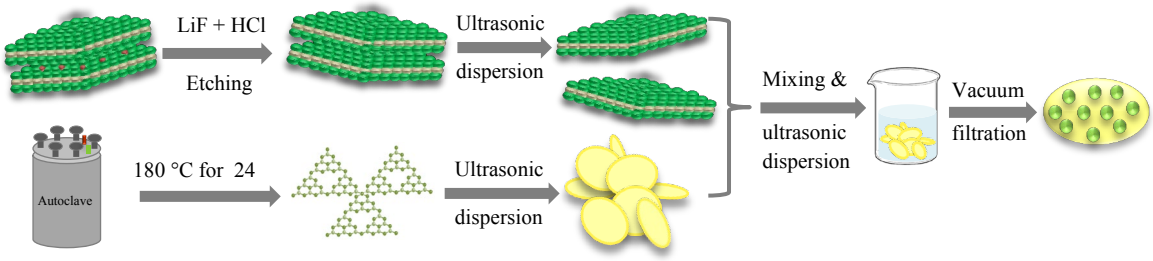

Fig. 6. Preparation process of g-C_3N_4/$Ti_3C_2T_x$ composite for fabrication membrane.

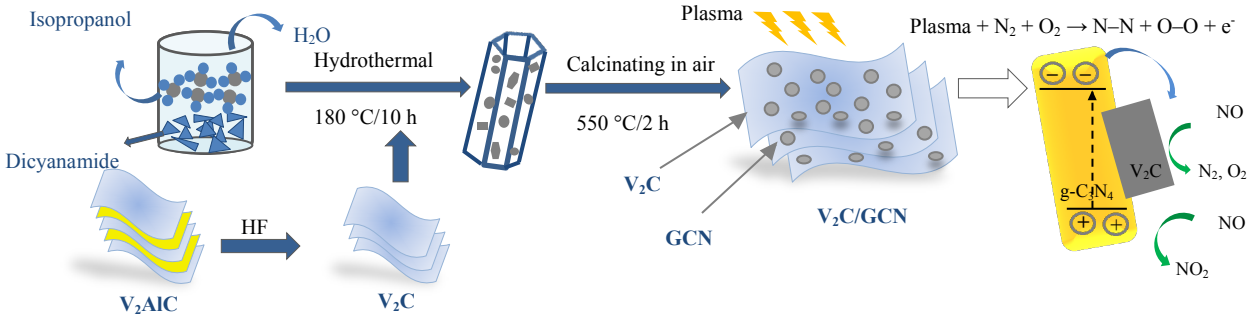

Fig. 7. Shematic illustration of V_2C/GCN fabrication via solvothermal method.

of dyes. Using this strategy, Liu and coworkers have synthesized Ti_3C_2/g-C_3N_4 composite through a simple sonochemical method in deionized water [56]. The close interfacial structure of g-C_3N_4/Ti_3C_2 assists in photogenerated charge transfer and enhances rates of pollutant degradation, CO_2 reduction, and N_2 fixation. Recently, Jin et al. have designed a supramolecular GCN/Ti_3C_2 Schottky junction composite via the sonicating method for the degradation of arbidol hydrochloride the most widely used drug against COVID-19 [57]. The Ti_3C_2 NSs have been fixed on supramolecular g-C_3N_4 NSs in the TEM image, presenting close contact between MXene and GCN. The transient photo-current response curve Ti_3C_2/supramolecular GCN exhibited enhanced photo-current response, which indicates a greater rapid separation rate of e^-/h^+ pairs on hybrid composite with extending the lifetime of charge carriers.

3.3. Simple mixing method

The simple mixing method is also used to fabricate g-C_3N_4/MXene composite, in which MXenes act as an auxiliary catalyst. For example, g-C_3N_4 has been decorated with alkalinized $Ti_3C_2(OH)_2$ via a mixing method for promoted photocatalytic performance [58]. Using this approach, quantitative $Ti_3C_2(OH)_2$ and g-C_3N_4 have been mixed and agitated in an aqueous solution. The obtained suspension has been centrifugally separated and then dried to be ground. This method is used as a common technique to accompany GCN and MXene with desired morphology. The PL spectra of g-C_3N_4/$Ti_3C_2(OH)_2$, using a UV–vis spectrophotometry show a light absorption edge of 475 nm, near the same for GCN. In another study, Xu et al. simply mixed plasma-treated $Ti_3C_2T_x$ MXene and GCN in a solution of water and isopropanol [59]. The TEM image of the sample has shown a layered attachment between GCN and plasma-treated $Ti_3C_2T_x$, like a sandwich structure. Besides, protonated g-C_3N_4/Ti_3C_2 has been designed by mixing method overnight and has been ground to a fine powder [60]. The SEM image of the GCN/Ti_3C_2 nanocomposite shows a smooth surface compared to the single GCN and MXene. Therefore, by pairing MXene and GCN, the surface morphology changes, and the range of light absorption increases. From the UV-visible spectroscopy and photoluminescence emission measurements, it can be found that the binary composite has a higher e^-/h^+ separation efficiency and provide more photogenerated charge carriers.

3.4. Hydro/solvothermal method

One of the powerful methods of preparing semiconductors is the hydro/solvothermal method, the advantages of which have been mentioned in the literature [61]. The hydrothermal method is similar to the solvothermal technique; only they are named based on whether the solvent is water or an organic solution. Hu et al. have used a solvothermal approach for the synthesis of V_2C/GCN employing 50 vol% isopropanol solution in distilled water, as shown in Fig. 7 [62]. Dicyanamide is dissolved in the initial alcoholic solution and stirred for a few minutes. Then it is mixed with V_2C and transferred to an autoclave and subjected to high temperature for several hours. Similarly, Yuan et al. synthesized 2D-2D MoS_2/GCN composite by solvothermal method. It is worth noting that by washing solid products several times with water and other solvents, the preparation process becomes longer [63]. The temperature and pressure inside the reaction vessel can be controlled [64]. After this period, in order to separate the phases, the obtained suspension is centrifuged. The filtration method can also be used to remove the liquid phase from intermediate materials [65]. The hydro/solvothermal method is widely used in the synthesis of nanomaterials, especially semiconductors [66, 67]. If needed, washing with water can be repeated several times to remove more alcohol left in the solid [68]. Afterwards, the calcination process takes place on the precursor with a constant heating rate. TGA analysis has shown that the photocatalyst obtained by the solvothermal method has higher thermal stability than g-C_3N_4 and V_2C. One of the advantages of the hydro/solvothermal method is the tunable morphology of the surfaces by controlling the reaction conditions [69–72]. In addition, by adjusting the pH during the solvent thermal technique, the generation of byproducts can be minimized or stopped [73].

3.5. Self-assembly method

Self-assembly is a useful technique in manufacturing complex composites based on coupling positively charged photocatalysts with negative species [74]. Due to the presence of end terminals in MXenes, negative surface charges create electrostatic attraction with positively charged photocatalysts. Hence, g-C_3N_4 can be hybridized with MXenes through the self-assembly method by adjusting the pH of the mixture [75]. In such a situation, Hu et al. prepared g-C_3N_4/Ti_3C_2 nanocomposite by an easy electrostatic self-assembly technique [76]. Ti_3C_2 colloid solution has been dropped in an ultrasonicated mixture of g-C_3N_4 and water followed by agitating, filtering, and drying. The elemental mapping analysis has confirmed the presence of titanium, carbon, and nitrogen in the sample and the layer-by-layer form of the composite has been clearly observed in the SEM images. In 2020, Song et al. employed the self-assembly method for fabricating a new $Ti_3C_2T_x$/V_c-CN (carbon vacancy C_3N_4) composite composed of

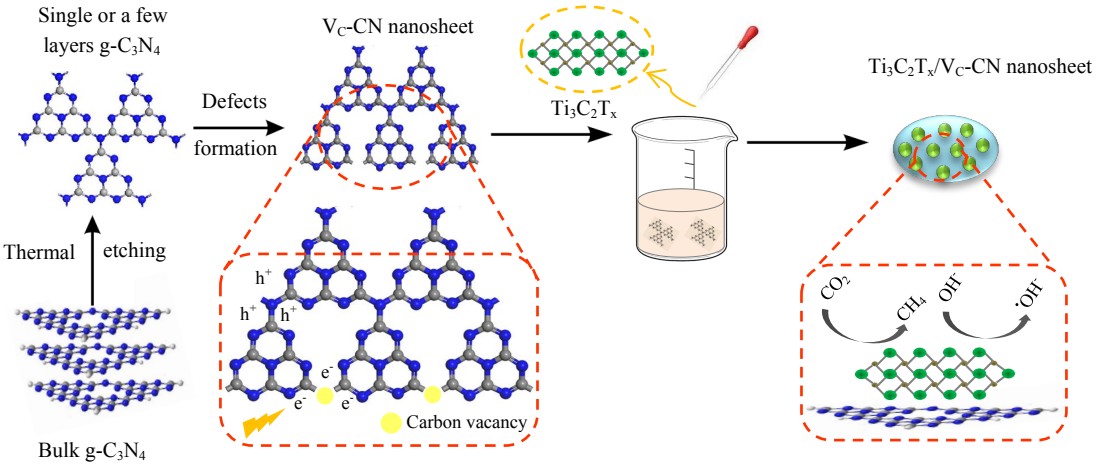

Fig. 8. Schematic route for preparing the Schottky junction of 2D/2D $Ti_3C_2T_x$/carbon vacancy C_3N_4.

modified defective GCN nanosheets and Ti_3C_2Tx, as shown in Fig. 8 [77]. The carbon vacancy facilitates the dissociation of the Frenkel exciton and the recombination of electrons and holes is somewhat debilitated. The EIS analysis showed that the e^-/h^+ transfer resistance of the fabricated composite is considerably lower than the same figure for the pure C_3N_4 sample, which proves that mixing these materials has played a significant role in increasing the conductivity of the photocatalyst. In similar research, the photocatalytic properties of Ti_3C_2 MXene/g-C_3N_4 toward H_2O_2 production were evaluated [78]. The transient photocurrent response revealed the positive effect of Ti_3C_2 on the composite and Ti_3C_2/g-C_3N_4 can reach a higher current density than bare porous C_3N_4. TC/PCN reach approximately 1 μA/cm^2, while the same figure for PCN was about 0.55 μA/cm^2. The self-assembled $Ti_3C_2T_x$ MXene/Graphitic Carbon Nitride composite has a 2D structure that provides a high surface area and can perform an excellent photocatalytic activity. Hence, Kang et al. designed $Ti_3C_2T_x$ hollow spheres together with protonated g-C_3N_4 using a sacrificial template via electrostatic layered assembly (Fig. 9a) [79]. Various analyzes indicate the positive effect of large contact between protonated g-C_3N_4 and 3D $Ti_3C_2T_x$ nanoshells on light absorption ability, surface area, and charge separation rate, which leads to improve the photocatalytic performance as shown in Fig. 9b, c.

In another research, a self-assembly technique induced by evaporation has been explored to fabricate Schottky heterojunction Ti_3C_2/g-C_3N_4 [80]. First melamine has been calcinated in a muffle furnace at 520 °C which was then grounded into small particles. Next, the prepared powder has been annealed for 2 h at about 520 °C. The Ti_3C_2 sheets have been fabricated similarly to the previous via HF etching solution. The Ti_3C_2 nanosheets have been mixed in water and sonicated for 4h. Then the prepared solution has been heated to evaporate the solvent

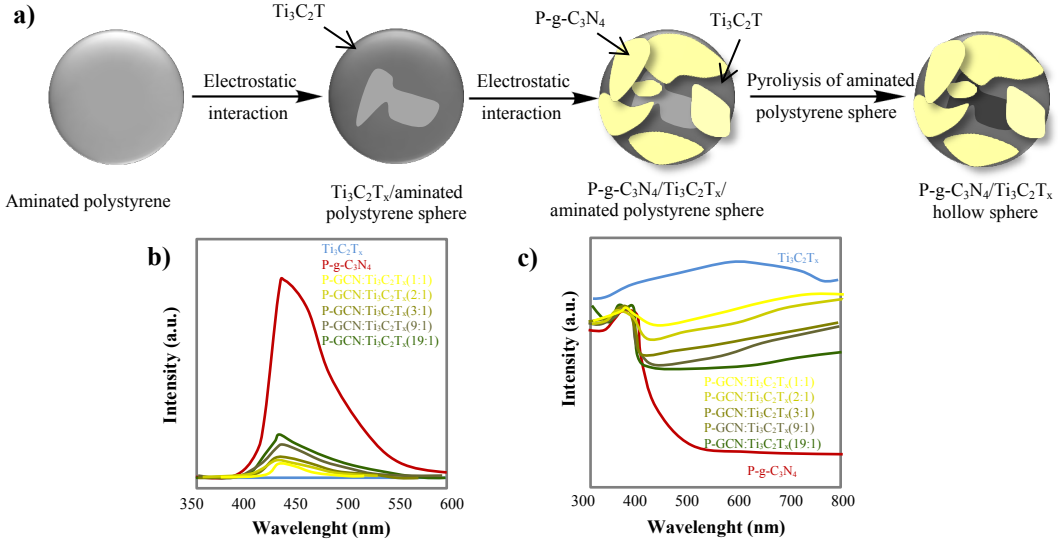

Fig. 9. a) Schematic representation of $Ti_3C_2T_x$/g-C_3N_4 fabrication in hollow form, b) photoluminescence spectroscopy image, and c) ultraviolet diffuse reflectance spectra.

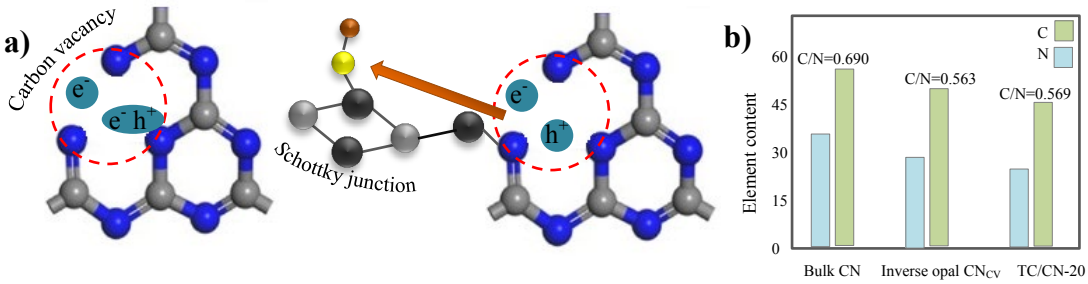

Fig. 10. a) Schematic representation of charge carriers behavior in C vacancy for inverse opal GCN_{CV} and b) elemental analysis pattern of bulk GCN, inverse opal GCN_{CV}, and TC/GCN-20.

completely. At last, freeze-drying has conducted to remove water from the structure. According to SEM images, 2D layers of the composite are clearly seen. In order to construct a 3D composite, Chang et al. created a Schottky junction between half-reduced Ti_3C_2 quantum dots (r-Ti_3C_2 QDs) on GCN spheres by electrostatic assembly [81]. To produce the C_3N_4 spheres, the Stöber method was employed using SiO_2@monodisperse SiO_2 spheres as a hard template [82]. By evaluating the photocurrent response of the synthesized catalysts it was revealed that the C_3N_4/r-Ti_3C_2 has higher charge transfer compared to C_3N_4. The higher photocurrent during light on-off cycles indicates the high number of photo-generated charge carriers. By comparing the optical current density in argon and nitrogen atmospheres, it can be observed that the optical current density is higher in argon because the electrons produced from photocatalysts are transferred to N_2 molecules. Hence, it is revealed that r-Ti_3C_2 QDs/GCN has a promising potential for photocatalytic nitrogen fixation under visible light radiation. Furthermore, He et al. confirmed the ability of photocatalytic degradation of diclofenac by Ti_3C_2/g-C_3N_4 composite prepared by ultrasonic-assisted self-assembly technique [83]. The TEM image of the as-prepared sample consists of 2D sheet-like nanostructure of both GCN and Ti_3C_2. The light absorption edge of pristine GCN at 476 nm has been characterized by UV-visible absorption spectra, while in the T/CN composite, the ability light absorption in both the visible and UV regions has increased. Later, Zhou et al. investigated 2D g-C_3N_4/Mo_2C structure and photocatalytic activity within pharmaceutical and personal care products degradation [84]. They prepared porous GCN_4 nanosheets/Mo_2C nanosheets via a simple electrostatic self-assembly technique. The photocurrent response curves show that the photocurrent density of GCN/Mo_2C is 1.5 times that of GCN. Therefore, it is clear that charge carriers are more effectively separated and transferred after combining with this type of MXene.

In another study, g-C_3N_4/Ti_3C_2 composite has been made and its photocatalytic activity toward H_2O_2 production has been studied [85]. The catalyst was fabricated using an electrostatic self-assembly technique by incorporating Ti_3C_2 QDs carbon vacancies into GCN. Elemental analysis (EA) identified the vacancy type after calcination, which proved that the C/N mole ratio of bulk CN is larger than that of GCN with carbon vacancies (Fig. 10). SEM images showed that the fabricated structure has numerous pores with a mean size of 200 nm which could result in a high surface area of the catalyst. By comparing the concentration of produced g-C_3N_4/Ti_3C_2 with bulk g-C_3N_4, it was found that the made composite has far better performance than the other one. In addition, Su et al. have studied 2D/2D GCN/Ti_3C_2 heterojunction nanosheets for hydrogen production under sunlight [86]. They have employed the electrostatic self-assembly technique to produce the catalyst. According to HRTEM images of the sample, the 2D/2D heterojunctions between Ti_3C_2 and GCN were successfully formed. Correspondingly, Wang et al. have designed a 2D/2D GCN/MXene composite for the oxidation of 5-hydroxymethylfurfural [87]. MXene nanosheets obtained by etching Ti_3AlC_2 with g-C_3N_4 synthesized according to the literature were ultrasonically dispersed. Then, Ti_3AlC_2/g-C_3N_4 composites have been prepared through a self-assembly procedure with different amounts of MXene. The FT-IR spectra confirmed that the MXeneX/GCN composite keeps pure phases of Ti_3C_2 and g-C_3N_4. HRTEM image analysis indicates well contact between 2D lattice MXene and 2D GCN. To demonstrate the application of MXenes in photocatalysis, Li et al. fabricated Ti_3C_2 QDs as a cocatalyst with g-C_3N_4 NSs via a self-assembly technique to form heterostructure for boosting photocatalytic H_2 evolution [88]. To prepare Ti_3C_2 QD/GCN composite, Ti_3C_2 solution has been mixed with g-C_3N_4 NSs, followed by freeze-drying. The BET surface area of the synthesized Ti_3C_2 QD@GCN composite is more evaluated than pure GCN nanosheets. The diameter of most mesopores is in the range of 2–25 nm. The presence of such nanopores facilitates photoinduced charge transfer [89]. Also, it is clear that the pore's diameter is relatively dependent on the loading amount of Ti_3C_2. Later, the ultrasonic-assisted self-assembly method has been used to prepare 2D/2D Mo_2C/GCN nanojunction photocatalyst [90]. From UV−vis absorption spectroscopy, it has been found that increasing the loading amount of Mo_2C affects the light absorption ability and expands the range of light spectrum absorption.

3.6. Wet impregnation method

Wet impregnation is one of the usual techniques to assemble g-C_3N_4-based composites with nanostructure morphology. In order to overcome the limitation of the MXenes and GCN interface, apply the construction of a 2D/2D heterojunction instead of a 0D/2D heterojunction. It is a high-efficient route because of much more contact areas, improving the electron migration rate, and decreasing the transfer distance and duration of photoinduced electrons to the photocatalyst surface. Recently, this strategy has been utilized for the design of heterostructure GCN/MXene to prohibit oxidizing $Ti_3C_2T_x$ by Nasri et al. [91]. Schottky junction and interfacial contact between both compounds enhance charge mobility and offer efficient photocatalytic performance. FESEM images of all samples loaded with different amounts of MXene show the encapsulation and intimate contact between Ti_3C_2 and GCN. The observed adsorption isotherm of the as-prepared sample highlights mesoporous hole sizing under 50 nm. The

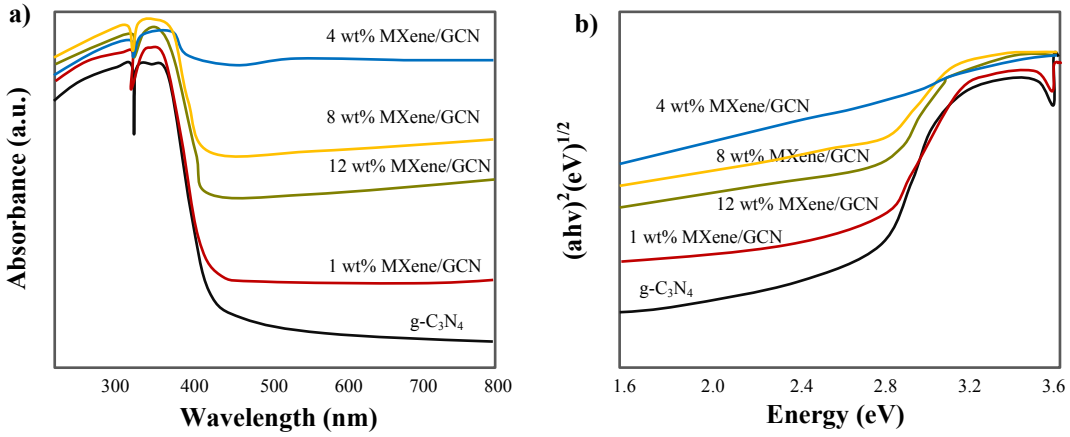

Fig. 11. a) UV-Vis diffuse reflection absorption spectra and b) Tauc curves of the as-synthesized MXene/GCN heterostructure photocatalysts.

BET-specific surface area, mesopore size, and content of the heterojunction system are successfully increased compared to the pure GCN and MXene. UV–vis spectrophotometer shows a stronger visible-light absorption capacity for MXene/g-C_3N_4 heterostructure (Fig. 11). In another research, a wet impregnation method has been applied to fabricate MXene/GCN composite with various amounts of MXene loading [92]. H_2O_2 has been introduced as a strong oxidizer during the photocatalysis experiment to enhance photocatalytic activity. TEM images of the as-synthesized samples indicate the successfully grown MXene on the surface of GCN with the development of binary MXene/GCN heterostructure.

3.7. Polymerization method

Thermal polymerization of urea to form GCN by introducing 2D Ti_3C_2 is a new strategy that results in increasing stability and recyclability due to the high-temperature process [93]. In a semi-closed system, NH_3 produced during g-C_3N_4 polymerization can prevent Ti_3C_2 oxidation by creating a reducing environment [94]. At high temperatures, a part of the surface functional groups (–OH, –O, and –F) attached to the end of Ti_3C_2 are separated, thereby increasing the interaction between GCN and Ti_3C_2. As a result of forming a stable heterostructure composite, the separation of charge carriers is accelerated and leads to the promotion of the photocatalytic reaction. In Fig. 12, the transient photocurrent responses show a larger ESI radius compared to the Ti_3C_2/GCN electrode, which indicates greater interface resistance and electron transfer ability. Li et al. designed a binary GCN/MXene composite by the thermal polymerization of cyanamide (CN_2H_2) and Ti_3C_2 in a nitrogen environment [95]. In the SEM image of the GCN/Ti_3C_2 photocatalyst, the layered form can hardly be seen, and CN strongly surrounds MXene. HRTEM image displays the low crystallinity of the GCN with obvious lattice fringes of Ti_3C_2. In addition, electrochemical impedance spectroscopy of GCN/Ti_3C_2 indicates a lower resistance of charge transfer compared to pristine GCN (Fig. 13).

3.8. In-situ growth method

In-situ growth is one of the polymerization methods where the polymer is formed directly on the surface of the particles. In fact, all polymerization occurs in the continuous phase. In this method, the polymer substrate is nanoparticles, and the monomer includes the filler particles during growth. Thermal polymerization by simple in-situ growth method is used to accompany GCN molecules and MXene nanoparticles. For example, urea and Ti_3C_2 powders are mixed in ethanol solution and heated in a muffler furnace after drying and grinding. Li et al. have reported the light response of g-C_3N_4/Ti_3C_2 nanocomposite is significantly improved due to the presence of metal in MXene [96]. The layered structure of Ti_3C_2 found in the SEM image revealed the in-situ growth of g-C_3N_4 on the surface of Ti_3C_2. Well-dispersed GCN NSs are seen on the thin Ti_3C_2 layers in the HRTEM image. Furthermore, the density functional theory (DFT) calculations have evidenced the interfacial interaction between GCN and MXene. The abundance of titanium element in Ti_3C_2 composition, hydrophilic end groups and excellent metal conductivity has made it preferable as an auxiliary catalyst over noble metals [97]. Later, heptazine-based C_3N_4 (H-CN)/Ti_3C_2 heterojunction photocatalyst has been constructed by an ionothermal in situ growth of h-C_3N_4 on ultrathin Ti_3C_2 NSs [98]. In this regard, melamine powder has been mixed with water followed by Ti_3C_2 added and dried in N_2. After pre-heating of suspension, the obtained solid has been ground with LiCl and KCl and afterward

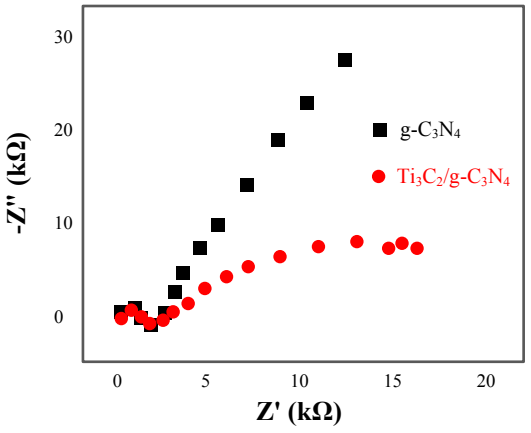

Fig. 12. Transient light current response of GCN and Ti_3C_2/GCN samples.

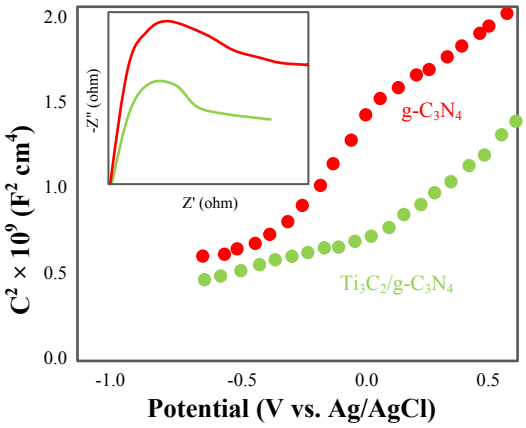

Fig. 13. Electrochemical impedance spectroscopy (EIS (c-inset)) of GCN/Ti_3C_2.

heated under an N_2 atmosphere. The final powder has been washed with hot water and dried. FESEM image of h-C_3N_4/Ti_3C_2 shows anchored MXene nanosheets with loose and ordered structures.

3.9. Annealing method

The annealing method is also used in the fabrication of Ti_3C_2/g-C_3N_4 nanocomposite while MXene powder is already prepared as an auxiliary catalyst. The annealing temperature is one of the most important operating factors because MXenes are sensitive to heat and oxidized to titania at high temperatures. Therefore, to maintain the resistance and conductivity of the composite, the temperature conditions must be controlled. In order to hybridize g-C_3N_4 and $Ti_3C_2T_x$, gray mesoporous GCN powder obtained from a mixture of melamine and urea in ethanol, with exfoliated $Ti_3C_2T_x$, has been directly heated at a constant annealing rate [99]. The surface morphology of the photocatalyst indicated that $Ti_3C_2T_x$ gets in intense contact with GCN. The adsorption and desorption isotherms in Fig. 14a show a slight decrease in the surface area of GCN/TC compared to pure GCN because of loaded $Ti_3C_2T_x$ which has a low surface area. The UV–Vis DRS spectrum in Fig. 14b displays a severe enhancement in the visible range absorption. In addition, Sun and coworkers prepared $Ti_3C_2T_x$/g-C_3N_4 composites through an annealing method in a furnace under N_2 protection or atmosphere to modify the Ti_3C_2 surface termination groups [100]. They found that the air-annealed sample had the highest Ti/F ratio, indicating a reduction in the number of fluorine terminals after the heat-treating process. Previously, it has also been reported that during the annealing process above 200 °C, the hydroxyl species on the surface of Ti_3C_2 are removed and Ti–O–Ti bonds appear [101, 102].

4. Photocatalytic applications of GCN/MXene composite

Incorporating MXenes into the g-C_3N_4 is an effective strategy to improve the photocatalytic performance of g-C_3N_4 and solar energy utilization efficiency, which is related to an increased photoresponse and a rapid separation rate of photoinduced charge carriers than pure g-C_3N_4. Their application mainly includes the H_2 evolution from water splitting, CO_2 reduction, wastewater treatment, N_2 fixation, and H_2O_2 generation. The performance of binary GCN/MXenes photocatalyst will be surveyed in the current section.

4.1. H_2 production

The replacement of traditional fossil fuels with alternative energy sources that have characteristics of eco-friendly and cleanliness, has received attention in recent years. Besides the radiolysis of water [103], photocatalytic production of hydrogen through water splitting can be a practical way to produce renewable energy without carbon dioxide emissions [104]. Among various composites, MXene/g-C_3N_4 has a significant potential to produce H_2 via photosplitting of water [105, 106]. Table 1 summarizes the conditions and results of MXene/GCN systems in hydrogen production.

Recently, Shao et al. indicated the performance of GCN during photocatalytic H_2 production have been improved using a cocatalyst of 2D Ti_2C MXenes at room temperature [47]. Under optimal conditions the rate of hydrogen generation with heterostructure Ti_2C/GCN system is much higher compared to pristine g-C_3N_4. Despite Ti_2C being a metallic compound, the H_2 production yield has been attributed to the formation of Ti_2CO_2 and TiO_2. In another approach, Li et al. fabricated heptazine-based C_3N_4 (H-CN) and Ti_3C_2 heterojunction by ionothermal method [98]. The experimental results and DFT calculation revealed that HCN/MXene composite had greater photocatalytic activity than single H-CN. The photoinduced charge carriers in HCN insulated from MXene nanosheets are more likely to recombine, leading to enhance H_2

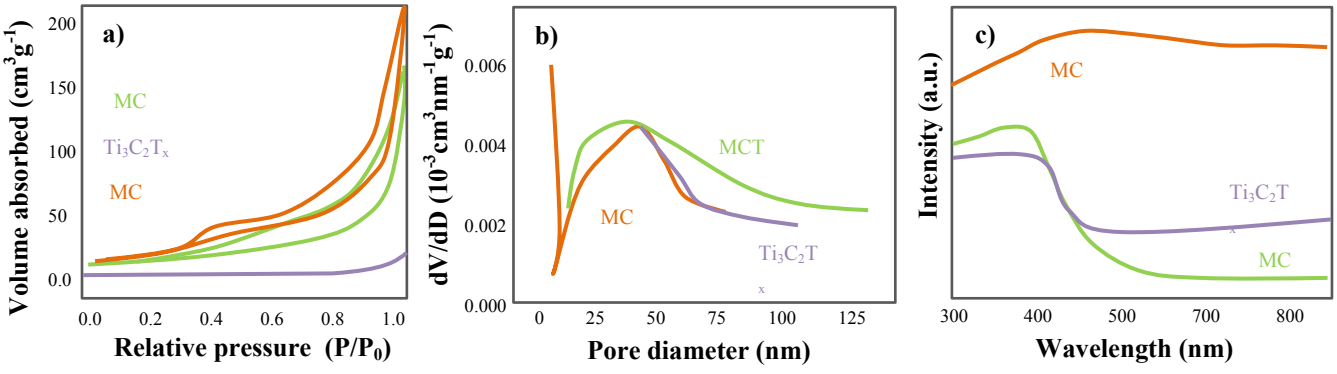

Fig. 14. a) N_2 adsorption–desorption isotherm curves, b) pore-size dispensation plots, and c) UV–Vis DRS spectrum.

Table 1. Summary of photocatalytic performance by use of MXene/g-C_3N_4 hybrid system in H_2 evolution.

Photocatalyst	Morphology	Synthesis method	Light source	Sacrificial agent	Condition	Activity ($\mu mol.g^{-1}.h^{-1}$)	Ref.
g-C_3N_4/Ti_3C_2	2D/3D heterojunction	In situ growth	300 W Xe lamp $\lambda > 420$ nm	TEOA	298 K, H_2 as gas carrier	116.2	[46]
Ti_2C/ g-C_3N_4	2D	Calcination	Monochromatic light, $\lambda > 420$ nm	TEOA	298 K, N_2 as gas carrier	950	[47]
g-C_3N_4/Mo_2C	1D heterostructure	Calcination	300 W Xe lamp $\lambda \geq 420$ nm	TEOA	277 K, N_2 as gas carrier	507	[50]
g-C_3N_4/p-$Ti_3C_2T_x$	2D/2D layered	Mechanical mixing	350 W Xe lamp $\lambda > 400$ nm	TEOA	298 K	17.8	[59]
g-C_3N_4/Ti_3C_2	2D nanosheet	In situ growth	300 W Xe lamp $\lambda > 420$ nm	TEOA	N_2 protection	727	[60]
MoS_2/g-C_3N_4	2D/2D nanosheet	Solvothermal	300 W xenon lamp, $\lambda \geq 420$ nm	TEOA	293 K, Ar as gas carrier	1155	[63]
p-g-C_3N_4/$Ti_3C_2T_x$	Hollow-sphere	Electrostatic assembly	300 W Xe lamp	TEOA	Ar as gas carrier	982.8	[79]
Ti_3C_2/g-C_3N_4	2D/2D heterojunction	Electrostatic self-assembly	200 W Hg lamp	TEOA	298 K, Ar as gas carrier	72.3	[86]
g-C_3N_4@Ti_3C_2	Quantum dots	Self-assembly	300 W Xe lamp	TEOA	H_2 atmosphere	5111.8	[88]
Mo_2C/g-C_3N_4	2D/2D	Self-assembly	300 Xe lamp $\lambda > 420$ nm	TEOA	277 K	675.27	[90]
Ti_3C_2/g-C_3N_4	2D/2D heterojunctions	Thermal polymerization	300 W Xe lamp $\lambda > 420$ nm,	TEOA	Ar as gas carrier	26.7	[94]
HCN/Ti_3C_2	Schottky heterojunction	In-situ growth	LED lamps λ=420 nm	TEOA	N_2 as gas carrier	4225	[98]
g-C_3N_4/$Ti_3C_2T_x$	2D	Annealing	350 W Xe lamp $\lambda > 400$ nm	TEOA	Ar as gas carrier	88	[100]

photocatalytic evolution performance. Similarly, Su et al. have reported that 2D/2D Ti_3C_2/g-C_3N_4 composites displayed 10 times higher photocatalytic H_2 evolution than pure GCN under visible spectrum [86]. The g-C_3N_4 photocatalytic activity increased due to the construction of 2D heterojunctions and intimate contact between nanolayer of GCN and MXene. Furthermore, the photoexcited electron transfer can be facilitated due to the super metallic conductivity of Ti_3C_2 and the Schottky junction structure of MXene and g-C_3N_4 composite. In another research, a 0D/2D Ti_3C_2/GCN composite was prepared by the embellishing of Ti_3C_2 MXene quantum dots (QDs) in order to boost GCN nanosheets for photocatalytic H_2 generation [88]. The results have showed that at optimized amounts of Ti_3C_2 QDs, the photocatalytic H_2 evolution efficiency of GCN/Ti_3C_2 quantum dots composite is higher than GCN/Ti_3C_2. The Q-dots of MXene can raise the BET and present more active sites which lead to highly efficient photocatalytic activity.

Correspondingly, Li et al. have prepared a unique form of 2D/3D GCN/Ti_3C_2 heterostructure through the uniform dispersion of GCN on the Ti_3C_2 surface [46]. Under visible light irradiation, the improved GCN/Ti_3C_2 photocatalyst displayed six times higher photocatalytic H_2 generation capacity than the pure GCN. $Ti_3C_2T_x$-based MXenes are proposed as efficient cocatalysts for photocatalytic H_2 production. Having functional groups such as hydroxyl (–OH) in $Ti_3C_2T_x$-based MXenes leads to hydrophilic behavior that can interact strongly with water molecules and facilitate the photocatalytic reaction. Sun et al. showed the annealing of carbon nitride and $Ti_3C_2T_x$ composite promotes photocatalytic activity [100]. The presence of the oxygen functional group improves the separation of electron-hole pairs and causes a 105% rise in hydrogen production. They also proved that oxygen surface termination enhances hydrogen evolution by DFT calculations. Xu et al. carried out the plasma treatment on the surface of g-C_3N_4/$Ti_3C_2T_x$ to enhance the photocatalytic activity of the catalyst for H_2 evolution [59]. Increasing the ratio of the Ti–O functional group, especially Ti^{4+}, helps to capture strongly photoinduced electron from GCN and significantly boost the separation of charge carriers. Kang et al. have made three-dimensional GCN/$Ti_3C_2T_x$ hollow spheres to raise the rate of photocatalytic hydrogen (H_2) evolution [79]. The structure in the optimization state indicated 3.5-fold and 1.22-fold higher H_2 production than g-C_3N_4 and gC_3N_4/$Ti_3C_2T_x$, which lack the hollow structure, respectively. Based on density functional theory (DFT), Liu et al. calculated the bandgap of 2D semiconductor Ti_2CO_2/g-C_3N_4. They found that the van der Waals type of heterostructure Ti_2CO_2@g-C_3N_4 has a lower bandgap compared to the bandgap of their pristine species [107]. The direct Z-scheme heterojunction in the Ti_2CO_2@GCN photocatalyst is created through the normal type II band alignment, which is the electron-hole transfer interface. It is notable that in all H_2 evolution experiments, TEOA was used as h^+ scavenger and oxidized to $TEOA^+$.

4.2. CO_2 reduction

The emission of tremendous and uninterrupted volumes of CO_2 into the atmosphere has led to the acute phenomenon of global warming. The photocatalytic process of CO_2 reduction, which is called the holy grail reaction, can overcome environmental problems and reduce greenhouse gases by converting CO_2 and H_2O directly into hydrocarbon fuels. However, the progress of photocatalytic CO_2 reduction is hampered by limitations such as slow charge formation, poor adsorption, and activation of carbon dioxide on the photocatalysts' surface. Two dimensional (2D) ultrathin g-C_3N_4 nanosheets are recently applied to improve the usage of sunlight and the adsorption of CO_2 to the photocatalytic system. Owing to its unique characteristics such as hydrophilic surface and active sites, MXenes are considered a group of materials that have advantages for carbon dioxide absorption in the photocatalytic system. The simultaneous use of MXene as cocatalysts with GCN promotes the photoconversion of CO_2. Tang et al. showed that the alkalinized 2D Ti_3C_2 MXene mixed with 2D g-C_3N_4 improved CO_2 reduction performance 5.9 times higher than that of pure g-C_3N_4 at the optimized composite [58]. The great electrical conductivity of MXene/GCN and the adsorption capacity of alkalized Ti_3C_2 are the reasons for its high efficiency.

Yang et al. created ultrathin 2D/2D Ti_3C_2/GCN heterostructure by calcination and mixing which displayed an 8.1 times larger CO_2 reduction rate than pure g-C_3N_4 [49]. Urea is responsible for making a gas template to exfoliate Ti_3C_2 into nanosheets and the precursor of g-C_3N_4 to craft Ti_3C_2/g-C_3N_4 heterojunction. Enhanced photocatalytic efficiency of 2D/2D Ti_3C_2/GCN nanocomposites have been originate from the formation of an ultrathin heterostructure, which creates an intimate interface contact between the GCN and MXene cocatalyst and transfers the conduction band electrons of GCN to the surface of MXene, separating the photoinduced electron/hole pairs. Hu et al. conducted the conjunction Ti_3C_2 (TC) on porous C_3N_4 (PCN) with rich –NH_x via NH_xTi bond [76]. Under visible light and at optimal conditions, CH_4 production was obtained 14 times greater than the pure PCN. Even after the four-cycle, the photocatalytic activity of the composite is acceptable. The main reason was attributed to the activation/absorption of CO_2 and boosting of light-harvesting ability. In addition, the presence of chemical bonding of NH_x-Ti and electrical conductivity makes it possible to separate and migrate interfacial surface charge. Li et al. fabricated mesoporous GCN/$Ti_3C_2T_x$ (MCT) that CH_4 production yielded 2.4 times more than GCN [99]. The porous structure provides more adsorption sites for carbon dioxide due to the large contact surface. Furthermore, the high-speed electron transport of the MXene simplified charge separation. Song et al. constructed a 2D/2D Schottky junction of GCN NSs photocatalyst with carbon vacancy which is modified by $Ti_3C_2T_x$. The synergy of promotion exciton dissociation into free charge through carbon vacancies in g-C_3N_4 and directional charge transfer led to the formation of an electron-accumulated catalytic surface which was made better CO evolution 7.4 times higher than pristine GCN [77]. Furthermore, Baghini and coworkers proposed GCN/Lu_2CF_2 and GCN/Y_2CF_2 Z-scheme composites to reach a highly significant photocatalytic CO_2 reduction under sunlight illumination [108]. They have found these MXenes have significant photoabsorption in the visible and ultraviolet regions and have proved monolayers of Lu_2CF_2 and Y_2CF_2 are promising candidates for photocatalytic reactions and solar energy. In another study, the photocatalytic reduction of CO_2 with V_2C/GCN binary composite has been tested by Madi et al. [109]. The highest efficiency has been achieved by controlled coupling of 15%-V_2C with g-C_3N_4 for CH_4 and CO generation.

4.3. Removal of pollutant

In the last few decades, a serious concern for the environment formed, which requires an immediate search for new strategies to solve the growing environmental problems [110, 111]. Pharmaceutical industries, antibiotics, personal care products and organic dyes introduce emerging pollutants into water sources that destroy human and aquatic health [112]. Photocatalytic degradation of environmental pollutants is a newly developed method in recent research. Semiconductor g-C_3N_4 and MXenes as catalyst supports have been designed to manufacture heterogeneous semiconductor photocatalytic systems with the motive of removing pollution. Table 2 shows a summary of MXene/GCN hybrid systems with the approach of removing pollutants.

Polymeric and photocatalytic membranes are newly considered as mixed matrix membranes in water purification [113]. In this regard, Zeng et al. prepared $Ti_3C_2T_x$/GCN 2D/2D photocatalytic membrane for the removal of dyes and antibiotics during wastewater treatment [55]. The pressure test through the experimental device revealed the significant permeable character of the as-synthesized sample. The penetrance of the membrane increases with the high content of GCN as shown in Fig. 15a. Furthermore, it was found that the Congo red (CR) and Trypan blue (TB) dyes degradation has reached the maximum values of 98% and 96%, respectively (Fig. 15b, c). In addition, the self-cleaning capability of the membrane was examined in the presence and absence of light. The experiment results indicated the great self-cleaning capability of $Ti_3C_2T_x$/g-C_3N_4 membrane in light without any washing process, which reduces chemical cleaning agents' needs. Also, the results demonstrated the membrane can remove up to 86% of tetracycline antibiotics under visible light. In another study, Zhou et al. evaluated the tetracycline degradation by Mo_2C/GCN Van der Waals heterostructure under visible spectrum [84]. They found the photocatalytic degradation activity enhanced with the increase of Mo_2C up to 2 wt%. Also, Mo_2C/g-C_3N_4 showed high recyclability and stability with little inhibition in photocatalytic performance after 4 rounds of continuous reactions. The degradation of arbidol hydrochloride (ABLH) as a Covid-19 drug has also been recently investigated by Jin and coworkers with Ti_3C_2/supramolecular g-C_3N_4 [57]. For this purpose, a novel Schottky junction photocatalyst has been evaluated to promote the oxidation pathway under visible light irradiation. The as-prepared photocatalyst with 0.5 wt% Ti_3C_2 showed 99.2% removal of ABLH from water within 120 minutes. The type of dissolved organic substances, anions (SO_4^{2-} and NO_3^-), and pH have a significant effect on photocatalytic activity. Besides, Dong et al. used Ti_3C_2/g-C_3N_4 composite to remove tetracycline hydrochloride under simulated light [94]. They showed that Ti_3C_2/GCN nanosheets can degrade tetracycline hydrochloride up to 84.5% within 2 h, while this figure is 29% for the single GCN. Similarly, Ti_3C_2/GCN was prepared and utillized to activate peroxymonosulfate for the decomposition of diclofenac in wastewater under sunlight irradiation [83]. The degradation test results showed that this photocatalyst can completely degrade diclofenac (100%) in alkaline solution (pH=10~11) with 0.21/min first-order kinetic constant (k).

Much research has been performed to achieve the photocatalytic degradation of dyes over GCN-based semiconductors. For example, Nasri et al. synthesized Ti_3C_2/GCN heterostructure photocatalyst and

Table 2. Summary of the g-C_3N_4/MXene systems used in pollutant removal.

Photocatalyst	Morphology	Synthesis method	Pollutant	Conditions	Light source	Irradiation time	Removal (%)	Ref.
$Ti_3C_2T_x$/ alkalized C_3N_4	Heterostructure	Calcination	Tetracycline hydrochloride	30 min stirring in the dark	300 W xenon lamp, $\lambda > 420$ nm	10 min	77%	[48]
Ti_3C_2/PCN	VDW heterostructure	Straightforward vacuum filtration	Phenol	30 min stirring in the dark	500 W xenon lamp, $\lambda > 420$ nm	180 min	Day 98% night 32%	[54]
g-C_3N_4@MXene	2D/2D nanosheets	Vacuum filtration	Congo red (CR), trypan blue (TB), TC-HCl	Exposure for 8 hours in a dark	Full-spectrum gold halogen lamp, 70 W	8 h	98% of CR 96% of TB 86% of TC	[55]
Ti_3C_2/g-C_3N_4	Schottky junction	Simple sonochemical	Levofloxacin	60 min stirring in the dark	300 W xenon lamp, $\lambda > 420$ nm	4 h	72%	[56]
TiC/SCN	Schottky junction	Simple method	Arbidol hydrochloride (ABLH)	30 min stirring in the dark	300 W xenon lamp, $420 < \lambda < 780$ nm	150 min	99.2%	[57]
g-C_3N_4/Ti_3C_2	2D/2D heterojunction	Self-assembly	Ciprofloxacin (CIP)	30 min stirring in the dark	500 W xenon light, $\lambda \geq 400$ nm	150 min	40%	[80]
Ti_3C_2/g-C_3N_4	2D/2D heterostructure	Self-assembly	Diclofenac (DCF)	30 min stirring in the dark	300W xenon lamp	30 min	95%	[83]
Mo_2C/g-C_3N_4	2D/2D VDW heterojunction	Electrostatic self-assembly	Tetracycline (TC)	60 min stirring in the dark	300 W xenon lamp, $\lambda \geq 420$ nm	60 min	97%	[84]
MXene/g-C_3N_4	Heterostructure	Wet impregnation	Methylene blue	60 min stirring in the dark	500 W halogen lamp	3 h	69.4%	[91]
Ti_3C_2/g-C_3N_4	2D multilayer	Wet impregnation	Methylene blue	Keeping at RT for 1 h, H_2O_2 oxidizer	Halogen lamp of 500 W	240 min	99.7%	[92]
Ti_3C_2/g-C_3N_4	2D/2D heterojunctions	Simple low-temperature treated	Tetracycline hydrochloride (TC-HCl)	30 min stirring in the dark	250 W xenon lamp, $\lambda \geq 420$ nm	2 h	79%	[94]
g-C_3N_4/ amorphous Ti-peroxo	Heterojunction	Electrostatic self-assembly	Rhodamine B, tetracycline (TC)	30 min stirring in the dark	270 W xenon lamp, $\lambda > 420$ nm	60 min	97.22% of RhB 86.34% of TC	[114]

evaluated its activity for methylene blue (MB) destruction [91]. The prepared 1 wt% Ti_3C_2/GCN heterostructure nanocomposite displayed the highest photocatalytic performance over 180 min. Doubtless, narrower bandgap energy, good crystallinity structures, and a high BET surface area are the most vital factors for enhancing photocatalytic efficiency. In another research, g-C_3N_4/Ti_3C_2 heterojunction photocatalyst has been designed for reduction of the MB concentration under H_2O_2 oxidizer [92]. To achieve maximum removal of the persistent dyes, 1 wt% Ti_3C_2/g-C_3N_4 could be the optimum content. Accordingly, Tu and coworkers successfully have applied Ti_3C_2-derived amorphous Ti-peroxo heterojunction coupled with GCN for rhodamine B (RhB) degradation [114]. Parameters such as initial pH, H_2O_2 dosage, and Ti_3C_2-Mxene content affect the photocatalytic activity. The presence of Ti-peroxo complex has displayed 97.9% RhB removal within 1 h under visible light illumination.

4.4. H_2O_2 production

Hydrogen peroxide (H_2O_2) is an environmentally friendly and versatile oxidizer whose only byproduct is water [115, 116]. It has wide applications such as water remediation, chemical processing, disinfection, and pulp industry [117, 118]. In recent years, hydrogen peroxide as an alternative to H_2 has attracted considerable attention as energy carrier in fuel cells [119, 120]. Semiconductor photocatalysis is supposed a desirable method to produce H_2O_2 due to its safety, energy conservation, and anti-pollution property. Reduction of O_2 to hydrogen peroxide is possible through photogenerated electrons on the conduction band of the semiconductor [121]. GCN has motivated vast research attention due to its physiochemical stability, economics, nontoxicity, appropriate band structure and visible light absorption. However, the use of g-C_3N_4 in the form of bulk morphology hinders its

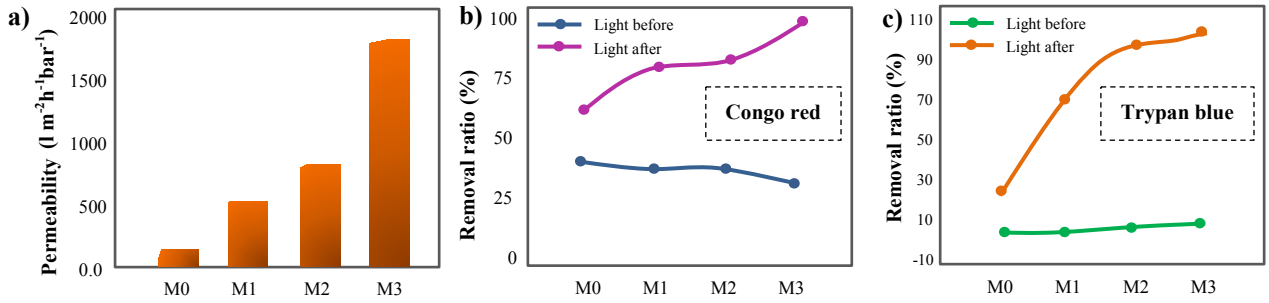

Fig. 15. a) Permeability of membranes with different GCN content and b, c) removal ratios of Congo red and Trypan blue from sewage by various membranes.

photocatalytic performance due to its small surface area and low photogenerated carrier separation and transfer efficiency. Therefore, researchers have developed various methods for g-C_3N_4 to improve its photocatalytic performance. Ti_3C_2 could be coupled with semiconductor photocatalysts to form Schottky junctions, which greatly promote the separation of photogenerated charge carriers. Yang et al. combined GCN with Ti_3C_2 through a simple electrostatic self-assembly method to accelerate the spatial charge carrier separation and activated molecular O_2 for H_2O_2 generation [78]. The increase in H_2O_2 production rate by 2.1 times more than the g-C_3N_4 is related to the formation of Schottky junction with the porous g-C_3N_4 and subsequent built-in electric field at the interface. Lin et al. constructed the Ti_3C_2 quantum dot-modified defective inverse opal g-C_3N_4 (TC/CN) to facilitate photocatalytic hydrogen peroxide generation [85]. Under visible light, the efficiency of H_2O_2 production at the optimum amount of TC/CN was 9.3 times larger than that of bulk CN which is ascribed to the direction-induced bonding between carbon vacancies in GCN and Ti_3C_2 quantum dots.

4.5. N_2 fixation

Elemental nitrogen is a vital component for the life of organisms on earth. Nitrogen (N_2) is present in abundance up to 78%, however its intrinsic inert, highly stable triple bond, and low solubility in water prevent its direct use in chemical processes. The conversion of N_2 to NH_3 is an important process for N_2 fixation. Until now, the powerful procedure of industrial ammonia synthesis is through the Haber process, which uses nitrogen and hydrogen as raw materials in the presence of iron and ruthenium metal catalysts. This reaction requires a large amount of energy input. It also emits a huge content of greenhouse gases into the atmosphere. The conversion of nitrogen to ammonia is kinetically complex. For this purpose, various catalytic methods have been proposed. The g-C_3N_4 photocatalyst can product ammonia under visible light spectrum due to its very negative conduction band position and moderate bandgap structure. However, the recombination rate of induced electron-hole pairs limits the photocatalytic activity of GCN in nitrogen conversion. MXenes have high specific conductance, which can combine effectively with GCN. For example, Liu et al. fabricated a TiO_2/C/GCN photocatalyst by thermal treatment of a mixture of $Ti_3C_2T_x$ and melamine [122]. This approach endows TiO_2-supported 2D carbon NSs with a large number of Ti^{3+} ions wrapped by in situ GCN NSs. TiO_2/C/GCN heterojunction shows a great photocatalytic NH_3 production rate 18 times higher than the pure GCN nanosheets under visible light irradiation. The Ti^{3+} ions as the active site adsorb nitrogen and also trap photoinduced electrons. Sun et al. indicated the high nitrogen conversion ability of N-defect GCN/Ti_3C_2 heterojunction composite synthesized by combination of nitrogen defect-rich GCN NSs with MXene [52]. This structure showed a considerable enhancement of photocatalytic activity rather than pristine Ti_3C_2 and gC_3N_4. This improvement is attributed to the induced N-defect and the heterostructure synergistically. Furthermore, the Ti element in Ti_3C_2 acts as the active surface for nitrogen adsorption and limits the H_2 evolution reactions instead. Accordingly, N_2 reduction was investigated by Ti_3C_2 MXene embellished g-C_3N_4 nanosheets in a quartz photochemical reactor at ambient conditions [56]. Ti_3C_2 MXene/g-C_3N_4 can break down the strong triple bond of N≡N to activate it for fixation. Ti_3C_2/g-C_3N_4 (x=1 wt%) displays the highest photocatalytic activity for NH^{4+} production, which reaches 600 μmol.l^{-1}.g_{cat}^{-1}.h^{-1}. In another study, Chang and coworkers designed surface defect-rich Ti_3C_2 QDs@ GCN hollow sphere for nitrogen fixation [81]. It was found that partially reduced Ti_3C_2 QDs-20 ml/GCN significantly improved NH^{4+} production under white light irradiation (660 μmol/l within 2 h).

4.6. NO purification

It is confirmed that nitric oxide (NO) leads to serious harm to the environment and human health. Photocatalytic oxidation is one of the useful methods because of its benefits for the environment. However, photocatalytic elimination of NO has some restrictions such as low process efficiency and by-product generation such as nitrogen dioxide, which are even more detrimental. For this purpose, constructing an efficient catalyst is the solution to overcome the photocatalytic oxidation problems of NO. Ti_3C_2 cocatalyst joined with GCN gathers the advantages of both which is a great strategy to improve NO conversion yield. Li et al. prepared Ti_3C_2/GCN system by a simple in-situ growing technique which improved the ratio of NO oxidation removal up to 57% compared to pure GCN [96]. It is worth noticing that the NO_2 fraction decreased to 8.7%. The DFT calculation revealed a short distance between oxygen and MXene (1.2 Å) than GCN leading to the priority adsorption of oxygen on MXene nanosheets. Therefore the more negative adsorption energy of oxygen is collected on MXene. In another research, photocatalytic denitrogenation of fuels over hybridized Ti_3C_2/GCN to obtain a Schottky barrier [53]. All Ti_3C_2 @GCN samples present increasing photocatalytic denitrogenation activity which is attributed to the intercalation between MXene and GCN. Accordingly, Hu and coworkers have successfully fabricated a new V_2C/g-C_3N_4 for plasma denitrification technology [62]. The optimized V_2C (3 wt%)/g-C_3N_4 exhibited an efficient NO removal of 83%, which is 2.1 and 1.2 folds higher than single GCN and V_2C.

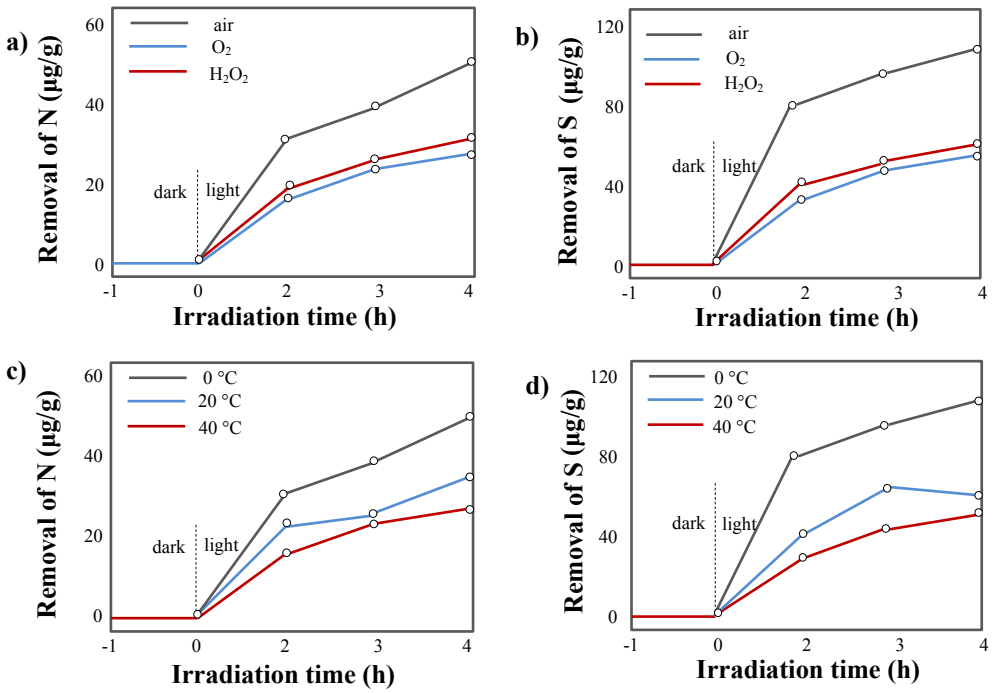

Fig. 16. Photocatalytic denitrogenation and desulfurization of a model fuel a, b) with different oxidants and c, d) over the different temperatures in the atmosphere.

4.7. Other applications

The photocatalytic redox reaction of chemical compounds is an efficient method to convert them into desired products. For example, the photo-reduction of uranium (VI) on the decorated GCN surface with Ti_3C_2 was investigated to separate from the aqueous solution and form forming UO_{2+x} ($x < 0.25$) deposits [95]. A solid-state Z-scheme heterostructure was figured because of the O–Ti–O formation on the surface of MXene, which enhanced the separation of charge carriers and facilitated charge carriers, and reduced U(VI) to U(IV). GCN/Ti_3C_2 (x=2) showed 14.05 times fold the reaction constant compared to pure GCN. The GCN/Ti_3C_2 composite has absorption light edge at about 500 to 800 nm while a single GCN weakly absorbs the visible spectrum in the region of ~450 nm. In another study, Li et al. worked on oxidative denitrogenation and desulfurization of fuels by Ti_3C_2/g-C_3N_4 composite in the atmosphere [53]. To produce model fuel and prepare N and S elements, pyridine and thiophene were dissolved in n-octane. It was seen that removal of the N and S elements increases in the atmosphere compared to using H_2O_2 or O_2 as oxidant as shown in Fig. 16. These species convert to OH and O_2 radicals under the reaction with electrons, which can boost the desulfurization and denitrogenation process. These species convert to $^{\bullet}OH$ and $^{\bullet}O_2$ radicals under the reaction with electrons, which can boost the desulfurization and denitrogenation process. Despite this, the extra H_2O_2 scrubs the $^{\bullet}OH$ radicals and prohibits sulfur and nitrogen oxidation. In addition, molecular O_2 in the atmosphere can play the role of an oxidant and reduce process costs.

5. Conclusions and outlook

Exploring the solar-driven photocatalyst for energy generation and environmental remediation led to sparked hybridization idea. The incorporation of g-C_3N_4 and MXenes is an exactly useful technique to uplift photocatalytic activity. This review summarized the advancement in the design and fabrication of 0D-2D, 1D-2D, 2D-2D, and 2D-3D GCN/MXene photocatalysts. The most common method of MXene/GCN nanocomposite synthesis is the electrostatic self-assembly technique and the calcination method is in the next order. Simple mixing and ultrasonic dispersion methods are also relatively popular compared to less common methods such as hydro/solvothermal. In the polymerization method, GCN is not used directly, but the raw material of GCN production during the formation of the polymer hybridized with MXene to form a composite.

High photocatalytic activity has been observed due to an effective association with g-C_3N_4 and MXenes. MXenes as cocatalyst and supporting material for g-C_3N_4 have been used in H_2 evolution, CO_2 conversion, N_2 photofixation, H_2O_2 generation, NO purification, pollutant elimination, decolorization and other application. Coupling of g-C_3N_4 with MXene results in an expanded light absorption spectrum, which will enlarge photogenerated electron/hole pairs. In addition, MXenes profoundly improve the Schottky barrier by forming a heterojunction structure that accelerates photoinduced charge carrier separation. The distance of electron immigration is shortened by the wide and intimate interfaces of GCN and MXene then facilitate the transfer and separation of charge carriers. Interfacial contact among GCN and MXenes provides electron trapping channels to reduce the electron/hole recombination rate and adequate charge transport under the visible sunlight spectrum. The visible-light-driven MXene/GCN possesses an appropriate energy bandgap construction, which can supply sufficient potential for redox reactions. The MXene/GCN exhibits higher photocatalytic performance compared to pure GCN and single MXene. In addition, MXenes are good candidates to replace expensive noble metal catalysts for g-C_3N_4. Although there are a few weaknesses and restrictions in the incorporated MXenes in GCN, the

MXene/GCN nanocomposite exhibits higher photocatalytic performance compared to pure GCN and single MXene. But the results obtained from photocatalysis show that there is still a long way to practical use of MXene/GCN.

CRediT authorship contribution statement

Asieh Akhoondi: Writing – original draft, Supervision.
Mehrdad Mirzaei: Writing – review & editing, Resources.
Mostafa Y. Nassar: Writing – review & editing.
Zahra Sabaghian: Writing – review & editing.
Farshid Hatami: Writing – review & editing.
Mohammad Yusuf: Writing – review & editing.

Data availability

As this is a review article, no new data were generated. All information is publicly available or cited appropriately within the article.

Declaration of competing interest

The authors declare no competing interests.

Funding and acknowledgment

This research received no external funding.

References

[1] D. Li, X. Fang, H. Liu, H. Lu, Z. Zhang, Photo reduction of CO2 to CH4 on g-C3N4: The effect of concentrating light and pretreatment, API Conf. Proc. 1971 (2018) 020006. https://doi.org/10.1063/1.5041101.
[2] J. Qi, W. Zhang, R. Cao, Solar-to-Hydrogen Energy Conversion Based on Water Splitting, Adv. Energy Mater. 8 (2018) 1701620. https://doi.org/10.1002/aenm.201701620.
[3] I. Dincer, Renewable energy and sustainable development: a crucial review, Renew. Sust. Energ. Rev. 4 (2000) 157–175. https://doi.org/10.1016/S1364-0321(99)00011-8.
[4] H. Frei, Photocatalytic fuel production, Curr. Opin. Electrochem. 2 (2017) 128–135. https://doi.org/10.1016/j.coelec.2017.03.009.
[5] H. Yan, J. Yang, G. Ma, G. Wu, X. Zong, et al., Visible-light-driven hydrogen production with extremely high quantum efficiency on Pt–PdS/CdS photocatalyst, J. Catal. 266 (2009) 165–168. https://doi.org/10.1016/j.jcat.2009.06.024.
[6] G. Zhang, C.D. Sewell, P. Zhang, H. Mi, Z. Lin, Nanostructured photocatalysts for nitrogen fixation, Nano energy. 71 (2020) 104645. https://doi.org/10.1016/j.nanoen.2020.104645.
[7] M. Bowker, Photocatalytic hydrogen production and oxygenate photoreforming, Catal. Lett. 142 (2012) 923–929. https://doi.org/10.1007/s10562-012-0875-4.
[8] J. Bi, B. Xu, L. Sun, H. Huang, S. Fang, et al., A cobalt-modified covalent triazine-based framework as an efficient cocatalyst for visible-light-driven photocatalytic CO2 reduction, ChemPlusChem. 84 (2019) 1149–1154. https://doi.org/10.1002/cplu.201900329.
[9] Z. Chen, D. Yao, C. Chu, S. Mao, Photocatalytic H2O2 production Systems: Design strategies and environmental applications, Chem. Eng. J. 451 (2023) 138489. https://doi.org/10.1016/j.cej.2022.138489.
[10] D. Chatterjee, S. Dasgupta, Visible light induced photocatalytic degradation of organic pollutants, J. Photochem. Photobiol. C. 6 (2005) 186–205. https://doi.org/10.1016/j.jphotochemrev.2005.09.001.
[11] K. Li, Y. He, P. Chen, H. Wang, J. Sheng, et al., Theoretical design and experimental investigation on highly selective Pd particles decorated C3N4 for safe photocatalytic NO purification, J. Hazard. Mater. 392 (2020) 122357. https://doi.org/10.1016/j.jhazmat.2020.122357.
[12] J. Fu, J. Yu, C. Jiang, B. Cheng, g-C3N4-Based Heterostructured Photocatalysts, Adv. Energy. Mater. 8 (2018) 1701503. https://doi.org/10.1002/aenm.201701503.
[13] L. Shi, Z. He, S. Liu, MoS2 quantum dots embedded in g-C3N4 frameworks: A hybrid 0D-2D heterojunction as an efficient visible-light driven photocatalyst, Appl. Surf. Sci. 457 (2018) 30–40. https://doi.org/10.1016/j.apsusc.2018.06.132.
[14] Z. Chen, T. Fan, M. Shao, X. Yu, Q. Wu, et al., Simultaneously enhanced photon absorption and charge transport on a distorted graphitic carbon nitride toward visible light photocatalytic activity, Appl. Catal. B. 242 (2019) 40–50. https://doi.org/10.1016/j.apcatb.2018.09.080.
[15] S. Cao, J. Yu, g-C3N4-based photocatalysts for hydrogen generation, J. Phys. Chem. Lett. 5 (2014) 2101–2107. https://doi.org/10.1021/jz500546b.
[16] M. Nemiwal, T.C. Zhang, D. Kumar, Recent progress in g-C3N4, TiO2 and ZnO based photocatalysts for dye degradation: Strategies to improve photocatalytic activity, Sci. Total Environ. 767 (2021) 144896. https://doi.org/10.1016/j.scitotenv.2020.144896.
[17] B. Xu, M.B. Ahmed, J.L. Zhou, A. Altaee, G. Xu, M. Wu, Graphitic carbon nitride based nanocomposites for the photocatalysis of organic contaminants under visible irradiation: Progress, limitations and future directions, Sci. Total Environ. 633 (2018) 546–559. https://doi.org/10.1016/j.scitotenv.2018.03.206.
[18] X. Yang, Y. Ye, J. Sun, Z. Li, J. Ping, X. Sun, Recent advances in g-C3N4-based photocatalysts for pollutant degradation and bacterial disinfection: Design strategies, mechanisms, and applications, Small. 18 (2022) 2105089. https://doi.org/10.1002/smll.202105089.
[19] E. Baladi, F. Davar, A. Hojjati-Najafabadi, Synthesis and characterization of g–C3N4–CoFe2O4–ZnO magnetic nanocomposites for enhancing photocatalytic activity with visible light for degradation of penicillin G antibiotic, Environ. Res. 215 (2022) 114270. https://doi.org/10.1016/j.envres.2022.114270.
[20] I. Tateishi, M. Furukawa, H. Katsumata, S. Kaneco, Photocatalytic degradation of bisphenol A using O-doped dual g-C3N4 under visible light irradiation, Catal. Today. 411–412 (2022) 113877. https://doi.org/10.1016/j.cattod.2022.08.019.
[21] L. Deng, J. Sun, J. Sun, X. Wang, T. Shen, et al., Improved performance of photosynthetic H2O2 and photodegradation by K-, P-, O-, and S-co-doped g-C3N4 with enhanced charge transfer ability under visible light, Appl. Surf. Sci. 597 (2022) 153586. https://doi.org/10.1016/j.apsusc.2022.153586.
[22] G. Gao, A.P. O'Mullane, A. Du, 2D MXenes: A New Family of Promising Catalysts for the Hydrogen Evolution Reaction, ACS Catal. 7 (2017) 494–500. https://doi.org/10.1021/acscatal.6b02754.
[23] K.R. Garrick Lim, A.D. Handoko, S.K. Nemani, B. Wyatt, H.-Y. Jiang, et al., Rational Design of Two-Dimensional Transition Metal Carbide/Nitride (MXene) Hybrids and Nanocomposites for Catalytic Energy Storage and Conversion, ACS Nano. 14 (2020) 10834–10864. https://doi.org/10.1021/acsnano.0c05482.
[24] M. Mansoorianfar, K. Shahin, A. Hojjati–Najafabadi, R. Pei, MXene–laden bacteriophage: A new antibacterial candidate to control bacterial contamination in water, Chemosphere. 290 (2022) 133383. https://doi.org/10.1016/j.chemosphere.2021.133383.
[25] M. Khazaei, M. Arai, T. Sasaki, C.-Y. Chung, N.S. Venkataramanan, et al., Novel electronic and magnetic properties of two-dimensional transition metal carbides and nitrides, Adv. Func. Mater. 23 (2013) 2185–2192. https://doi.org/10.1002/adfm.201202502.
[26] B.C. Wyatt, A. Rosenkranz, B. Anasori, 2D MXenes: Tunable Mechanical and Tribological Properties, Adv. Mater. 33 (2021) 2007973. https://doi.org/10.1002/adma.202007973.

[27] P. Kuang, Z. Ni, J. Yu, J. Low, New progress on MXenes-based nanocomposite photocatalysts, Mater. Rep: Energy. 2 (2022) 100081. https://doi.org/10.1016/j.matre.2022.100081.
[28] Y. Gogotsi, B. Anasori, The Rise of MXenes, ACS Nano. 13 (2019) 8491–8494. https://doi.org/10.1021/acsnano.9b06394.
[29] A. Hojjati-Najafabadi, M. Mansoorianfar, T. Liang, K. Shahin, Y. Wen, et al., Magnetic-MXene-based nanocomposites for water and wastewater treatment: A review, J. Water Process. Eng. 47 (2022) 102696. https://doi.org/10.1016/j.jwpe.2022.102696.
[30] H. Fang, Y. Pan, M. Yin, L. Xu, Y. Zhu, C. Pan, Facile synthesis of ternary Ti3C2–OH/ln2S3/CdS composite with efficient adsorption and photocatalytic performance towards organic dyes, J. Solid State Chem. 280 (2019) 120981. https://doi.org/10.1016/j.jssc.2019.120981.
[31] O. Salim, K.A. Mahmoud, K.K. Pant, R.K. Joshi, Introduction to MXenes: synthesis and characteristics, Mater. Today Chem. 14 (2019) 100191. https://doi.org/10.1016/j.mtchem.2019.08.010.
[32] R.T. Ginting, H. Abdullah, V. Fauzia, Facile preparation of MXene and protonated-g-C3N4 on natural latex foam for highly efficient solar steam generation, Matter. Lett. 313 (2022) 131779. https://doi.org/10.1016/j.matlet.2022.131779.
[33] P. Srinivasan, S. Samanta, A. Krishnakumar, J. Bosco Balaguru Rayappan, K. Kailasam, Insights into g-C3N4 as a chemi-resistive gas sensor for VOCs and humidity – a review of the state of the art and recent advancements, J. Mater. Chem. A. 9 (2019) 10612–10651. https://doi.org/10.1039/D0TA12500H.
[34] M. Shi, P. Xiao, J. Lang, C. Yan, X. Yan, Porous g-C3N4 and MXene Dual-Confined FeOOH Quantum Dots for Superior Energy Storage in an Ionic Liquid, Adv. Sci. 7 (2020) 1901975. https://doi.org/10.1002/advs.201901975.
[35] J. Pang, R.G. Mendes, A. Bachmatiuk, L. Zhao, H.Q. Ta, et al., Applications of 2D MXenes in energy conversion and storage systems, Chem. Soc. Rev. 48 (2019) 72–133. https://doi.org/10.1039/C8CS00324F.
[36] X. Yu, W. Yin, T. Wang, Y. Zhang, Decorating g-C3N4 Nanosheets with Ti3C2 MXene Nanoparticles for Efficient Oxygen Reduction Reaction, Langmuir. 35 (2019) 2909–2916. https://doi.org/10.1021/acs.langmuir.8b03456.
[37] X. Ma, Z. Ma, H. Zhang, D. Lu, J. Duan, B. Hou, Interfacial Schottky junction of Ti3C2Tx MXene/g-C3N4 for promoting spatial charge separation in photoelectrochemical cathodic protection of steel, J. Photochem. Photobiol. A. 426 (2022) 113772. https://doi.org/10.1016/j.jphotochem.2022.113772.
[38] A. Alaghmandfard, K. Ghandi, A Comprehensive Review of Graphitic Carbon Nitride (g-C3N4)–Metal Oxide-Based Nanocomposites: Potential for Photocatalysis and Sensing, Nanomater. 12 (2022) 294. https://doi.org/10.3390/nano12020294.
[39] J. Wen, J. Xie, X. Chen, X. Li, A review on g-C3N4-based photocatalysts, Appl. Surf. Sci. 391 (2017) 72–123. http://dx.doi.org/10.1016/j.apsusc.2016.07.030.
[40] L.C. Makola, S. Moeno, C.N.M. Ouma, A. Sharma, D.-V.N. Vo, L.N. Dlamini, Facile fabrication of a metal-free 2D–2D Nb2CTx@g-C3N4 MXene-based Schottky-heterojunction with the potential application in photocatalytic processes, J. Alloys Compd. 916 (2022) 165459. https://doi.org/10.1016/j.jallcom.2022.165459.
[41] C. Yuan, Z. He, Q. Chen, X. Wang, C. Zhai, M. Zhu, Selective and efficacious photoelectrochemical detection of ciprofloxacin based on the self-assembly of 2D/2D g-C3N4/Ti3C2 composites, Appl. Surf. Sci. 539 (2021) 148241. https://doi.org/10.1016/j.apsusc.2020.148241.
[42] Y.-P. Zhu, Y. Lei, F. Ming, E. Abou-Hamad, A.-H. Emwas, et al., Heterostructured MXene and g-C3N4 for high-rate lithium intercalation, Nano Energy. 65 (2019) 104030. https://doi.org/10.1016/j.nanoen.2019.104030.
[43] L. Wan, Y. Tang, L. Chen, K. Wang, J. Zhang, et al., In-situ construction of g-C3N4/Mo2CTx hybrid for superior lithium storage with significantly improved Coulombic efficiency and cycling stability, Chem. Eng. J. 410 (2021) 128349. https://doi.org/10.1016/j.cej.2020.128349.
[44] F. Liu, A. Zhou, J. Chen, J. Jia, W. Zhou, et al., Preparation of Ti3C2 and Ti2C MXenes by fluoride salts etching and methane adsorptive properties, Appl. Surf. Sci. 416 (2017) 781–789. https://doi.org/10.1016/j.apsusc.2017.04.239.
[45] D. Wang, J. Si, S. Lin, R. Zhang, Y. Huang, et al., Achieving Macroscopic V4C3Tx MXene by Selectively Etching Al from V4AlC3 Single Crystals, Inorg. Chem. 59 (2020) 3239–3248. https://doi.org/10.1021/acs.inorgchem.9b03625.
[46] J. Li, L. Zhao, S. Wang, J. Li, G. Wang, J. Wang, In situ fabrication of 2D/3D g-C3N4/Ti3C2 (MXene) heterojunction for efficient visible-light photocatalytic hydrogen evolution, Appl. Surf. Sci. 515 (2020) 145922. https://doi.org/10.1016/j.apsusc.2020.145922.
[47] M. Shao, Y. Shao, J. Chai, Y. Qu, M. Yang, et al., Synergistic effect of 2D Ti2C and g-C3N4 for efficient photocatalytic hydrogen production, J. Mater. Chem. A. 5 (2017) 16748–16756. https://doi.org/10.1039/C7TA04122E.
[48] X. Yi, J. Yuan, H. Tang, Y. Du, B. Hassan, et al., Embedding few-layer Ti3C2Tx into alkalized g-C3N4 nanosheets for efficient photocatalytic degradation, J. Colloid Interface Sci. 571 (2020) 297–306. https://doi.org/10.1016/j.jcis.2020.03.061.
[49] C. Yang, Q. Tan, Q. Li, J. Zhou, J. Fan, et al., 2D/2D Ti3C2 MXene/g-C3N4 nanosheets heterojunction for high efficient CO2 reduction photocatalyst: Dual effects of urea, Appl. Catal. B. 268 (2020) 118738. https://doi.org/10.1016/j.apcatb.2020.118738.
[50] J. Zhang, M. Wu, B. He, R. Wang, H. Wang, Y. Gong, Facile synthesis of rod-like g-C3N4 by decorating Mo2C co-catalyst for enhanced visible-light photocatalytic activity, Appl. Surf. Sci. 470 (2019) 565–572. https://doi.org/10.1016/j.apsusc.2018.11.165.
[51] K. He, J. Xie, Z.Q. Liu, N. Li, X. Chen, et al., Multi-functional Ni3C cocatalyst/g-C3N4 nanoheterojunctions for robust photocatalytic H2 evolution under visible light, J. Mater. Chem. A. 6 (2018) 13110–13122. https://doi.org/10.1039/C8TA03048K.
[52] C. Sun, Z. Chen, J. Cui, K. Li, H. Qu, et al., Site-exposed Ti3C2 MXene anchored in N-defect g-C3N4 heterostructure nanosheets for efficient photocatalytic N2 fixation, Catal. Sci. Technol. 11 (2021) 1027–1038. https://doi.org/10.1039/D0CY01955K.
[53] B. Li, H. Song, F. Han, L. Wei, Photocatalytic oxidative desulfurization and denitrogenation for fuels in ambient air over Ti3C2/g-C3N4 composites under visible light irradiation, Appl. Catal. B. 269 (2020) 118845. https://doi.org/10.1016/j.apcatb.2020.118845.
[54] N. Liu, N. Lu, H. Yu, S. Chen, X. Quan, Efficient day-night photocatalysis performance of 2D/2D Ti3C2/Porous g-C3N4 nanolayers composite and its application in the degradation of organic pollutants, Chemosphere. 246 (2020) 125760. https://doi.org/10.1016/j.chemosphere.2019.125760.
[55] G. Zeng, Z. He, T. Wan, T. Wang, Z. Yang, et al., A self-cleaning photocatalytic composite membrane based on g-C3N4@MXene nanosheets for the removal of dyes and antibiotics from wastewater, Sep. Purif. Technol. 292 (2022) 121037. https://doi.org/10.1016/j.seppur.2022.121037.
[56] W. Liu, M. Sun, Z. Ding, B. Gao, W. Ding, Ti3C2 MXene embellished g-C3N4 nanosheets for improving photocatalytic redox capacity, J. Alloys Compd. 877 (2021) 160223. https://doi.org/10.1016/j.jallcom.2021.160223.
[57] D. Jin, Y. Lv, D. He, D. Zhang, Y. Liu, et al., Photocatalytic degradation of COVID-19 related drug arbidol hydrochloride by Ti3C2 MXene/supramolecular g-C3N4 Schottky junction photocatalyst, Chemosphere. 308 (2022) 136461. https://doi.org/10.1016/j.chemosphere.2022.136461.
[58] Q. Tang, Z. Sun, S. Deng, H. Wang, Z. Wu, Decorating g-C3N4 with alkalinized Ti3C2 MXene for promoted photocatalytic CO2 reduction performance, J. Colloid Interface Sci. 564 (2020) 406–417. https://doi.org/10.1016/j.jcis.2019.12.091.

[59] F. Xu, D. Zhang, Y. Liao, G. Wang, X, Shi, et al., Synthesis and photocatalytic H2-production activity of plasma-treated Ti3C2Tx MXene modified graphitic carbon nitride, J. Am. Ceram. Soc. 103 (2020) 849–858. https://doi.org/10.1111/jace.16798.
[60] H. Xu, R. Xiao, J. Huang, Y. Jiang, C. Zhao, X. Yang, In situ construction of protonated g-C3N4/Ti3C2 MXene Schottky heterojunctions for efficient photocatalytic hydrogen production, Chin. J. Catal. 42 (2021) 107–114. https://doi.org/10.1016/S1872-2067(20)63559-8.
[61] A. Akhoondi, M. Aghaziarati, N. Khandan, Hydrothermal production of nano pyrite, 1st International Regional Chemical and Petroleum Engineering. (2010).
[62] H. Hu, R. Zhao, X. Fan, J. Liu, Y. Nie, D. Wang, Preparation of a novel V2C mxene/g-C3N4 and its performance in plasma catalytic denitrification, Int. Conf. Power Grid Sys. Green Energy (PGSGE). 252 (2021) 02068. https://doi.org/10.1051/e3sconf/202125202068.
[63] Y.-J. Yuan, Z. Shen, S. Wu, Y. Su, L. Pei, et al., Liquid exfoliation of g-C3N4 nanosheets to construct 2D-2D MoS2/g-C3N4 photocatalyst for enhanced photocatalytic H2 production activity, Appl. Catal. B. 246 (2019) 120–128. https://doi.org/10.1016/j.apcatb.2019.01.043.
[64] A. Akhoondi, M. Ziarati, N. Khandan, Hydrothermal Production of Highly Pure Nano Pyrite in a Stirred Reactor, Iran. J. Chem. Chem. Eng. 33 (2014) 15–19. https://doi.org/10.30492/IJCCE.2014.7189.
[65] B.P. Kafle, Introduction to nanomaterials and application of UV–Visible spectroscopy for their characterization, Chemical Analysis and Material Characterization by Spectrophotometry, Elsevier. (2020) 147–198. https://doi.org/10.1016/B978-0-12-814866-2.00006-3.
[66] P. Shafiee, M. Reisi Nafchi, S. Eskandarinezhad, S. Mahmoudi, E. Ahmadi, Sol-gel zinc oxide nanoparticles: advances in synthesis and applications, Synth. Sinter. 1 (2021) 242–254. https://doi.org/10.53063/synsint.2021.1477.
[67] A. Akhoondi, M. Aghaziarati, N. Khandan, Thermal Treatment on Synthesized Nano Pyrite, NTC2011. (2011).
[68] Y.X. Gan, A.H. Jayatissa, Z. Yu, X. Chen, M. Li, Hydrothermal Synthesis of Nanomaterials, J. Nanomater. 2020 (2020) 8917013. https://doi.org/10.1155/2020/8917013.
[69] Q. Zhang, L. Gao, Preparation of Oxide Nanocrystals with Tunable Morphologies by the Moderate Hydrothermal Method: Insights from Rutile TiO2, Langmuir. 19 (2003) 967–971. https://doi.org/10.1021/la020310q.
[70] A. Akhoondi, M. Aghaziarati, N. Khandan, Nano pyrite production by hydrothermal method and marcasite removal using sodium bicarbonate, Nanotechnology Iranian Student Conference. (2012).
[71] L. Ndlwana, N. Raleie, K.M. Dimpe, H.F. Ogutu, E.O. Oseghe, et al., Sustainable Hydrothermal and Solvothermal Synthesis of Advanced Carbon Materials in Multidimensional Applications: A Review, Materials. 14 (2021) 5094. https://doi.org/10.3390/ma14175094.
[72] R.-C. Xie, J.K. Shang, Morphological control in solvothermal synthesis of titanium oxide, J. Mater. Sci. 42 (2007) 6583–6589. https://doi.org/10.1007/s10853-007-1506-0.
[73] A. Akhoondi, M. Aghaziarati, N. Khandan, Production of highly pure iron disulfide nanoparticles using hydrothermal synthesis method, Appl. Nanosci. 3 (2013) 417–422. https://doi.org/10.1007/s13204-012-0153-1.
[74] W.-J. Ong, L.-L. Tan, S.-P. Chai, S.-T. Yong, A.R. Mohamed, Surface charge modification via protonation of graphitic carbon nitride (g-C3N4) for electrostatic self-assembly construction of 2D/2D reduced graphene oxide (rGO)/g-C3N4 nanostructures toward enhanced photocatalytic reduction of carbon dioxide to methane, Nano Energy. 13 (2015) 757–770. https://doi.org/10.1016/j.nanoen.2015.03.014.
[75] J. Wen, J. Xie, X. Chen, X. Li, A review on g-C3N4-based photocatalysts, Appl. Surf. Sci. 391 (2017) 72–123. https://doi.org/10.1016/j.apsusc.2016.07.030.
[76] J. Hu, J. Ding, Q. Zhong, Ultrathin 2D Ti3C2 MXene Co-catalyst anchored on porous g-C3N4 for enhanced photocatalytic CO2 reduction under visible-light irradiation, J. Colloid Interface Sci. 582 (2021) 647–657. https://doi.org/10.1016/j.jcis.2020.08.047.
[77] Q. Song, J. Hu, Y. Zhou, Q. Ye, X. Shi, et al., Carbon vacancy-mediated exciton dissociation in Ti3C2Tx/g-C3N4 Schottky junctions for efficient photoreduction of CO2, J. Colloid Interface Sci. 623 (2022) 487–499. https://doi.org/10.1016/j.jcis.2022.05.064.
[78] Y. Yang, Z. Zeng, G. Zeng, D. Huang, R. Xiao, et al., Ti3C2 Mxene/porous g-C3N4 interfacial Schottky junction for boosting spatial charge separation in photocatalytic H2O2 production, Appl. Catal. B. 258 (2019) 117956. https://doi.org/10.1016/j.apcatb.2019.117956.
[79] J. Kang, S. Byun, S. Kim, J. Lee, M. Jung, et al., Design of Three-Dimensional Hollow-Sphere Architecture of Ti3C2Tx MXene with Graphitic Carbon Nitride Nanoshells for Efficient Photocatalytic Hydrogen Evolution, ACS Appl. Energy Mater. 3 (2020) 9226–9233. https://doi.org/10.1021/acsaem.0c01590.
[80] N. Liu, N. Lu, Y. Su, P. Wang, Q. Quan, Fabrication of g-C3N4/Ti3C2 composite and its visible-light photocatalytic capability for ciprofloxacin degradation, Sep. Purif. Technol. 211 (2019) 782–789. https://doi.org/10.1016/j.seppur.2018.10.027.
[81] B. Chang, Y. Guo, H. Liu, L. Li, B. Yang, Engineering a surface defect-rich Ti3C2 quantum dots/mesoporous C3N4 hollow nanosphere Schottky junction for efficient N2 photofixation, J. Mater. Chem. A. 10 (2022) 3134–3145. https://doi.org/10.1039/D1TA09941H.
[82] T. Zhang, Q. Zhang, J. Ge, J. Goebl, M. Sun, et al., A Self-Templated Route to Hollow Silica Microspheres, J. Phys. Chem. C. 113 (2009) 3168–3175. https://doi.org/10.1021/jp810360a.
[83] J. He, J. Yang, F. Jiang, P. Liu, M. Zhu, Photo-assisted peroxymonosulfate activation via 2D/2D heterostructure of Ti3C2/g-C3N4 for degradation of diclofenac, Chemosphere. 258 (2020) 127339. https://doi.org/10.1016/j.chemosphere.2020.127339.
[84] Y. Zhou, C. Zhang, D. Huang, W. Wang, Y. Zhai, et al., Structure defined 2D Mo2C/2Dg-C3N4 Van der Waals heterojunction: Oriented charge flow in-plane and separation within the interface to collectively promote photocatalytic degradation of pharmaceutical and personal care products, Appl. Catal. B. 301 (2022) 120749. https://doi.org/10.1016/j.apcatb.2021.120749.
[85] S. Lin. N. Zhang, F. Wang, J. Lei, L. Zhou, et al., Carbon Vacancy Mediated Incorporation of Ti3C2 Quantum Dots in a 3D Inverse Opal g-C3N4 Schottky Junction Catalyst for Photocatalytic H2O2 Production, ACS Sustain. Chem. Eng. 9 (2021) 481–488. https://doi.org/10.1021/acssuschemeng.0c07753.
[86] T. Su, Z.D. Hood, M. Naguib, L. Bai, S. Luo, et al., 2D/2D heterojunction of Ti3C2/g-C3N4 nanosheets for enhanced photocatalytic hydrogen evolution, Nanoscale. 11 (2019) 8138–8149. https://doi.org/10.1039/C9NR00168A.
[87] X.-X. Wang, S. Meng, S. Zhang, X. Zheng, S. Chen, 2D/2D MXene/g-C3N4 for photocatalytic selective oxidation of 5-hydroxymethylfurfural into 2,5-formylfuran, Catal. Commun. 147 (2020) 106152. https://doi.org/10.1016/j.catcom.2020.106152.
[88] Y. Li, L. Ding, Y. Guo, Z. Liang, H. Cui, J. Tian, Boosting the Photocatalytic Ability of g-C3N4 for Hydrogen Production by Ti3C2 MXene Quantum Dots, ACS Appl. Mater. Interfaces. 11 (2019) 41440–41447. https://doi.org/10.1021/acsami.9b14985.
[89] J. Zhang, L. Qian, W. Fu, J. Xi, Z. Ji, Alkaline-Earth Metal Ca and N Codoped TiO2 with Exposed {001} Facets for Enhancing Visible Light Photocatalytic Activity, J. Am. Ceram. Soc. 97 (2014) 2615–2622. https://doi.org/10.1111/jace.12957.
[90] W. Liu, D. Zhang, R. Wang, Z. Zhang, S. Qiu, 2D/2D Interface Engineering Promotes Charge Separation of Mo2C/g-C3N4 Nanojunction Photocatalysts for Efficient Photocatalytic Hydrogen Evolution, ACS Appl. Mater. Interfaces. 14 (2022) 31782–31791. https://doi.org/10.1021/acsami.2c03421.
[91] M.S.I. Nasri, M.F.R. Samsudin, A.A. Tahir, S. Sufian, Effect of MXene Loaded on g-C3N4 Photocatalyst for the Photocatalytic

Degradation of Methylene Blue, Energies. 15 (2022) 955. https://doi.org/10.3390/en15030955.
[92] M.S.I. Nasri, M. Zulfiqar, M.F.R. Samsudin, S. Sufian, Photo-Fenton Oxidation and Adsorption Performance of MXene/G-C3N4 Heterostructures Under H2O2 Oxidizer: Experimental & Modeling Approach, SSRN. http://dx.doi.org/10.2139/ssrn.4136268.
[93] Y. Xie, M. Naguib, V.N. Mochalin, M.W. Barsoum, Y. Gogotsi, et al., Role of Surface Structure on Li-Ion Energy Storage Capacity of Two-Dimensional Transition-Metal Carbides, J. Am. Chem. Soc. 136 (2014) 6385–6394. https://doi.org/10.1021/ja501520b.
[94] H. Dong, X. Zhang, Y. Zuo, N. Song, X. Xin, et al., 2D Ti3C2 as electron harvester anchors on 2D g-C3N4 to create boundary edge active sites for boosting photocatalytic performance, Appl. Catal. A. 590 (2020) 117367. https://doi.org/10.1016/j.apcata.2019.117367.
[95] S. Li, Y. Wang, J. Wang, J. Liang, Y. Li, P. Li, Modifying g-C3N4 with oxidized Ti3C2 MXene for boosting photocatalytic U(VI) reduction performance, J. Mol. Liq. 346 (2022) 117937. https://doi.org/10.1016/j.molliq.2021.117937.
[96] J. Li, Q. Zhang, Y. Zou, Y. Cao, W. Cui, et al., Ti3C2 MXene modified g-C3N4 with enhanced visible-light photocatalytic performance for NO purification, J. Colloid Interface Sci. 575 (2020) 443–451. https://doi.org/10.1016/j.jcis.2020.04.119.
[97] J. Ran, G. Gao, F.-T. Li, T.-Y. Ma, A. Du, S.-Z. Qiao, Ti3C2 MXene co-catalyst on metal sulfide photo-absorbers for enhanced visible-light photocatalytic hydrogen production, Nat. Commun. 8 (2017) 28045015. https://doi.org/10.1038/ncomms13907.
[98] J. Li, J. Li, C. Wu, Z. Li, L. Cai, et al., Crystalline carbon nitride anchored on MXene as an ordered Schottky heterojunction photocatalyst for enhanced visible-light hydrogen evolution, Carbon. 179 (2021) 387–399. https://doi.org/10.1016/j.carbon.2021.04.046.
[99] X. Li, Y. Bai, X. Shi, J. Huang, K. Zhang, et al., Mesoporous g-C3N4/MXene (Ti3C2Tx) heterojunction as a 2D electronic charge transfer for efficient photocatalytic CO2 reduction, Appl. Surf. Sci. 546 (2021) 149111. https://doi.org/10.1016/j.apsusc.2021.149111.
[100] Y. Sun, D. Jin, Y. Sun, X. Meng, Y. Gao, et al., g-C3N4/Ti3C2Tx (MXenes) composite with oxidized surface groups for efficient photocatalytic hydrogen evolution, J. Mater. Chem. A. 6 (2018) 9124–9131. https://doi.org/10.1039/C8TA02706D.
[101] M.A. Hope, A.C. Forse, K.J. Griffith, M.R. Lukatskaya, M. Ghidiu, et al., NMR reveals the surface functionalisation of Ti3C2 MXene, Phys. Chem. Chem. Phys. 18 (2016) 5099–5102. https://doi.org/10.1039/C6CP00330C.
[102] Z. Li, L. Wang, D. Sun, Y. Zhang, B. Liu, et al., Synthesis and thermal stability of two-dimensional carbide MXene Ti3C2, Mater. Sci. Eng. B. 191 (2015) 33–40. https://doi.org/10.1016/j.mseb.2014.10.009.
[103] G. Imanova, Molecular hydrogen production by radiolysis of water on the surface of nano-ZrO2 under the influence of gamma rays, Synth. Sinter. 2 (2022) 9–13. https://doi.org/10.53063/synsint.2022.21105.
[104] G.A. Naikoo, H. Salim, T. Awan, I.U. Hassan, M.A. Tabook, et al., Recent trends in MXenes hybrids as efficient 2D materials for photo- and electrocatalysis hydrogen production, Mater. Today Chem. 26 (2022) 101108. https://doi.org/10.1016/j.mtchem.2022.101108.
[105] V.Q. Hieu, T.C. Lam, A. Khan, T.-T. Thi Vo, T.Q. Nguyen, et al., TiO2/Ti3C2/g-C3N4 ternary heterojunction for photocatalytic hydrogen evolution, Chemosphere. 285 (2021) 131429. https://doi.org/10.1016/j.chemosphere.2021.131429.
[106] X. An, W. Wang, J. Wang, H. Duan, J. Shi, X. Yu, The synergetic effects of Ti3C2 MXene and Pt as co-catalysts for highly efficient photocatalytic hydrogen evolution over g-C3N4, Phys. Chem. Chem. Phys. 20 (2018) 11405–11411. https://doi.org/10.1039/C8CP01123K.
[107] X.Liu, W.Kang, L.Qi, J.Zhao, Two-dimensional g-C3N4/Ti2CO2 heterostructure as a direct Z-scheme photocatalyst for water splitting: A hybrid density functional theory investigation, Phys. E: Low-Dimens. Syst. Nanostructures. 134 (2021) 114872. https://doi.org/10.1016/j.physe.2021.114872.
[108] Z. Khorasani Baghini, A. Mostafaei, M. Abbasnejad, Y2CF2 and Lu2CF2 MXenes under applied strain: Electronic, optical, and photocatalytic properties, J. Alloys Compd. 922 (2022) 166198. https://doi.org/10.1016/j.jallcom.2022.166198.
[109] M. Madi, M. Tahir, Z.Y. Zakaria, 2D/2D V2C mediated porous g-C3N4 heterojunction with the role of monolayer/multilayer MAX/MXene structures for stimulating photocatalytic CO2 reduction to fuels, J. CO2 Util. 65 (2022) 102238. https://doi.org/10.1016/j.jcou.2022.102238.
[110] L. Biswal, S. Nayak, K. Parida, Recent progress on strategies for the preparation of 2D/2D MXene/g-C3N4 nanocomposites for photocatalytic energy and environmental applications, Catal. Sci. Technol. 11 (2021) 1222–1248. https://doi.org/10.1039/D0CY02156C.
[111] M. Mansoorianfar, H. Nabipour, F. Pahlevani, Y. Zhao, Z. Hussain, et al., Recent progress on adsorption of cadmium ions from water systems using metal-organic frameworks (MOFs) as an efficient class of porous materials, Environ Res. 214 (2022) 114113. https://doi.org/10.1016/j.envres.2022.114113.
[112] H. Hou, G. Shao, W. Yang, Recent advances in g-C3N4-based photocatalysts incorporated by MXenes and their derivatives, J. Mater. Chem. A. 9 (2021) 13722–13745. https://doi.org/10.1039/D1TA02527A.
[113] I. Salahshoori, A. Seyfaee, A. Babapoor, Recent advances in synthesis and applications of mixed matrix membranes, Synth. Sinter. 1 (2021) 1–27. https://doi.org/10.53063/synsint.2021.116.
[114] W. Tu, Y. Liu, M. Chen, Y. Zhou, Z. Xie, et al., Carbon nitride coupled with Ti3C2-Mxene derived amorphous Ti-peroxo heterojunction for photocatalytic degradation of rhodamine B and tetracycline, Colloids Surf. A: Physicochem. Eng. 640 (2022) 128448. https://doi.org/10.1016/j.colsurfa.2022.128448.
[115] S. Li, G. Dong, R. Hailili, L. Yang, Y. Li, et al., Effective photocatalytic H2O2 production under visible light irradiation at g-C3N4 modulated by carbon vacancies, Appl. Catal. B. 190 (2016) 26–35. https://doi.org/10.1016/j.apcatb.2016.03.004.
[116] H. Hou, X. Zeng, X. Zhang, Production of Hydrogen Peroxide by Photocatalytic Processes, Angew. Chem. Int. Ed. 59 (2020) 17356–17376. https://doi.org/10.1002/anie.201911609.
[117] W. Xiong, Z. Zeng, G. Zeng, Z. Yang, R. Xiao, et al., Metal-organic frameworks derived magnetic carbon-αFe/Fe3C composites as a highly effective adsorbent for tetracycline removal from aqueous solution, Chem. Eng. J. 374 (2019) 91–99. https://doi.org/10.1016/j.cej.2019.05.164.
[118] K. He, G. Chen, G. Zeng, A. Chen, Z. Huang, et al., Three-dimensional graphene supported catalysts for organic dyes degradation, Appl. Catal. B. 228 (2018) 19–28. https://doi.org/10.1016/j.apcatb.2018.01.061.
[119] S. Zhao, T. Guo, X. Li, T. Xu, B. Yang, X. Zhao, Carbon nanotubes covalent combined with graphitic carbon nitride for photocatalytic hydrogen peroxide production under visible light, Appl. Catal. B. 224 (2018) 725–732. https://doi.org/10.1016/j.apcatb.2017.11.005.
[120] M. Cheng, Y. Liu, D. Huang, C. Lai, G. Zeng, et al., Prussian blue analogue derived magnetic Cu-Fe oxide as a recyclable photo-Fenton catalyst for the efficient removal of sulfamethazine at near neutral pH values, Chem. Eng. J. 362 (2019) 865–876. https://doi.org/10.1016/j.cej.2019.01.101.
[121] X. Li, P. Xu, M. Chen, G. Zeng, D. Wang, et al., Application of silver phosphate-based photocatalysts: Barriers and solutions, Chem. Eng. J. 366 (2019) 339–357. https://doi.org/10.1016/j.cej.2019.02.083.
[122] Q. Liu, L. Ai, J. Jiang, MXene-derived TiO2@C/g-C3N4 heterojunctions for highly efficient nitrogen photofixation, J. Mater. Chem. A. 6 (2018) 4102–4110. https://doi.org/10.1039/C7TA09350K.